THE ASTROPHYSICAL JOURNAL, 370:455–473, 1991 April 1

THE SURFACE BRIGHTNESS TEST FOR THE EXPANSION OF THE UNIVERSE. III. REDUCTION OF DATA FOR THE SEVERAL BRIGHTEST GALAXIES IN CLUSTERS TO STANDARD CONDITIONS AND A FIRST INDICATION THAT THE EXPANSION IS REAL

ALLAN SANDAGE[1]
The Observatories of the Carnegie Institution of Washington, 813 Santa Barbara Street, Pasadena, CA 91101-1292
AND
JEAN-MARC PERELMUTER[2]
H. Rowland Department of Physics and Astronomy, The Johns Hopkins University, Homewood Campus, Baltimore, MD 21218
Received 1990 July 5; accepted 1990 September 14

ABSTRACT

Petrosian radii, effective radii, apparent magnitudes, and average surface brightnesses are obtained for the first few ranked galaxies in 56 nearby clusters and groups using data from the literature. The radii of first-ranked galaxies continue to increase faster than Hubble's constant surface brightness scaling law of $M \sim -5 \log R$, steepening the variation of $\langle SB \rangle$ with M calibrated in Paper II. The strong correlation of $\langle SB \rangle$ with M (and consequently with R) makes the correction of $\langle SB \rangle$ data to "standard conditions" for the first few ranked cluster galaxies even more important than discussed in Paper II in a search for the Tolman SB effect to test the reality of the expansion.

A Scott-like selection bias is present in the data we have used, causing the first-ranked galaxies in our sample to have brighter absolute magnitudes at larger redshifts. This creates an *artificial* correlation of $\langle SB \rangle$ with $\log (1 + z)$ that imitates the Tolman cosmological surface brightness dimming with redshift but with a 4 times larger amplitude than is expected from theory if the universe expands. The correlation is shown to be an artifact of the selection biases in the sample.

It is demonstrated that biases of this kind can always be removed by reducing the $\langle SB \rangle$ values to a "standard condition" of either fixed M or fixed R by using the correlations calibrated here. We apply these reduction procedures to data on distant clusters obtained by Djorgovski and Spinrad and show that a strong Tolman-like signal is present that matches the required slope of $\langle SB \rangle / d \log (1 + z) \sim 10$ for an expanding manifold. Reasons are given to be cautious of the result despite its importance in justifying the standard model of cosmology by proving that the expansion is real. The conclusion from the present result, if confirmed, is that the conventional interpretation of the redshifts as a change of the cosmological metric scale factor with time is correct.

Subject headings: cosmology — galaxies: clustering — galaxies: photometry

1. INTRODUCTION

In the first paper of this series (Sandage & Perelmuter 1990a, hereafter SPI) we reviewed the Tolman test for the reality of the expansion. The surface brightness (hereafter SB) of a "standard source" decreases with increasing redshift as $(1 + z)^4$ if the scale factor of the metric changes with time. On the other hand, if the manifold is stationary, the SB should vary with redshift only as $(1 + z)$. Recall also that the Tolman $(1 + z)^4$ factor in the expanding case is independent of the deceleration parameter q_0, and therefore of the curvature (Sandage 1961, 1988c).

If the expansion is real, the received flux is decreased by one factor of $(1 + z)$ because the energy of each photon is reduced by the redshift, no matter what its cause. A second factor of $(1 + z)$ is due to the stretching of the path length, diluting the reception rate of the photons at the detector. In the older literature these two terms are called the "energy effect" and the "number effect," respectively. The decrease in the flux due to redshift in the expanding case is then $(1 + z)^2$, in contrast to $(1 + z)$ in the stationary case where only the "energy effect" operates.

Consider next the effect of redshift on the apparent area of the source. If the expansion is real, the observed area is increased by $(1 + z)^2$ due to what is sometimes called the "aberration" term for each of the two dimensions. On the other hand, no "aberration" is present in a stationary manifold. (The rigorous derivation of the area factor by Tolman 1930, 1934 and by Kristian & Sacks 1968 is deeper than simple aberration, but a classical derivation based on aberration gives the correct answer, besides giving a heuristic appreciation). Surface brightness, which is the flux per unit area, is therefore decreased by the two factors of $(1 + z)$ in the area and two factors of $(1 + z)$ in the flux, giving the Tolman surface brightness $(1 + z)^4$ factor for a true expansion.

The practical problems to be solved before making the Tolman test are (1) defining an operational method to obtain a metric radius over which to average the observed flux in real galaxies where SB varies by a factor of at least 1000 over the image, and (2) understanding the various effects other than the Tolman factor that can change the observed $\langle SB \rangle$, complicat-

[1] Member of the faculty of the Department of Physics and Astronomy of The Johns Hopkins University and Visiting Research Associate of the Space Telescope Science Institute, Baltimore, MD, between 1986 and 1989 when the initial part of this work was done.

[2] Space Telescope Science Institute Student Fellow during the early part of this work.

ing attempts to detect the Tolman effect if it is present. These include (1) evolution of both radius and luminosity in the look-back time, and (2) the variation of $\langle SB \rangle$ in any sample of even local galaxies due to its strong dependence on absolute magnitude and on linear radius in E galaxies. Such "extraneous" effects appear either as noise on the Tolman signal or as systematic biases due to selection effects or to evolution. The natural variation of $\langle SB \rangle$ with M and/or R requires, thereby, the reduction of observational data to "standard conditions" of either fixed M or fixed R.

In Paper I we discussed operational methods of obtaining practical measures of metric radii. These include both the "effective" radius and various Petrosian radii. We also discussed various evolutionary effects and showed that the predicted change of $\langle SB \rangle$ due to "passive evolution" from normal stellar evolution is smaller than the Tolman factor. Furthermore, the available data (Sandage 1988c for a review) show that "active" evolution in E galaxies is not expected until beyond redshifts of $z = 0.5$, and, even then, many E galaxies show no sign of active evolution at redshifts as large as 0.8 (Hamilton 1985). Furthermore, in other studies it has been argued (Oemler 1987; Arimoto 1989) that neither kind of evolution has appreciable effects on $\langle SB \rangle$ in the redshift range of interest here.

In Paper II (Sandage & Perelmuter 1990b, hereafter SPII) we discussed the dependence of $\langle SB \rangle$ on absolute magnitude and linear radii for E galaxies in five independent samples. These results followed the prior discovery of the dependence of SB on effective radius by Oemler (1974, 1976) and by Kormendy (1977). The correlations of $\langle SB \rangle$ with both absolute magnitude (M) and linear radii (R) provide the means to reduce observed $\langle SB \rangle$ values to the "standard conditions" of either fixed M or fixed R. These corrections are the subject of this paper.

Using different data we extend the results of Paper II to the first few ranked cluster E galaxies in a large sample of relatively nearby clusters ($z < 0.1$). The galaxies used here are generally brighter and larger than those studied in Paper II. Therefore, the parameter space explored in this paper encompasses the range of M and R expected for the first few ranked cluster galaxies at the large redshifts that must be used in any future application of the Tolman test.

The photometric data are given in § 2. From these data the correlations between $\langle SB \rangle$ and both M and R are shown in § 3. A selection effect that imitates a Tolman signal in these very local data but which is an artifact of the sample is discussed in § 4. The correction procedures developed in this series are applied to the high-redshift galaxy sample of Djorgovski & Spinrad (1981) in § 5 where a well-defined Tolman signal appears in the data. Although this would seem to be a strong proof that the universe expands and therefore that the conventional interpretation of the redshift is correct, the reliability of the conclusion is cautioned. A discussion is given in the final section of how to optimize the Tolman test in future observational programs.

2. THE PHOTOMETRIC DATA

2.1. *Reduction Procedure*

The data used here are the surface photometry of galaxies in nearby clusters from measurements by Oemler (1976), Thuan & Romanishin (1981), Malumuth & Kirshner (1985), and Schombert (1986, 1987). Oemler provided tables of his radial profiles in a number of clusters including Coma (used in Paper II), Perseus, and A779. Schombert provided a machine-readable tape for the data from his large study of bright cluster galaxies.

Following the methods in SPI and SPII, we have calculated the $m(r)$ growth curve and the Petrosian $\eta(r)$ curve for each of the 250 galaxies in our initial sample. These functions were calculated by integrating the tabulated $I(r)$ surface brightness profile using a circular integration aperture as justified in SPII. The listed $I(r)$ profiles from the literature were generally given in the V photometric band.

In a way described in SPII we have tested for systematic errors in the zero points of our calculation of $m(r)$ caused by (1) the neglect of flattening for non-E0 galaxies, (2) errors in the zero points of the listed $I(r)$ profiles, and (3) occasional uncertainties in the literature as to the exact bandpass used in the initial observations (i.e., Johnson V or B or Thuan-Gunn g, etc.). The method of zero-point correction was to compare our calculated $m(r)$ growth curve with the run of independently available photoelectric aperture values such as are shown in Figure 1 of Paper II. Literature sources for the external independent aperture photometry were (*a*) the catalogs of Longo & de Vaucouleurs (1983, 1985), Sandage (1972a, 1975), Hoessel, Gunn, & Thuan (1980, hereafter HGT), Schneider, Gunn, & Hoessel (1983, hereafter SGH),[3] Thuan & Romanishin (1981) already mentioned, Schild & Davis (1979), and van den Bergh (1978, 1988).

After inspecting our final data for the more than 250 galaxies in the Schombert (1987, Table 1) compilation, we have retained only those galaxies for which we have the external zero-point check of our calculated $m(r)$ curve for at least one member of the cluster. Our final sample, restricted in this way, contains 146 galaxies in 56 clusters. We made this restriction because we found that inclusion of galaxies with no external photometric zero-point check only increased the scatter of the correlations without affecting their overall morphology.

2.2. *The Data*

The Petrosian $\eta(r)$ function for each galaxy, operationally defined in SPI and calculated here from the adopted data, was read to obtain the angular metric radii $r''(\eta)$ at various η values. The magnitude inside each η radius was read from the $m(r)$ curve at the designated $r(\eta)$ values and was corrected for any zero-point error as explained above. The average SB over a circle of radius $r''(\eta)$ was then calculated from $r''(\eta)$ and the corrected $m(\eta)$ value.

The effective (half-light) photometric parameters were also determined from the same calculated and corrected $m(r)$ curve, extrapolated to $r = \infty$ using an appropriate template growth curve from the Oemler family (see SPI). The effective radius, read from the corrected $m(r)$ curve at the magnitude $V_T + 0.75$, when combined with V_e gives the effective mean surface brightness $\langle SB \rangle_e$.

The galaxies are identified in Table 1 by the Abell (1958)

[3] Aperture photometry is not listed in HGT or in SGH, nor are their data on the V photometric system. Rather they are given on the Thuan & Gunn (1976) intermediate band g system. To use their published data we have converted the g magnitudes to V by subtracting 0.18 mag from g (V is brighter than g). Furthermore, their listed photometry is the magnitude inside their "standard" metric radius of 16 kpc, calculated from some adopted growth curve of magnitude with angular radius. To make the conversion of angular size to a radius of 16 kpc they used a linear velocity-distance relation, a Hubble constant of $H_0 = 60$ km s^{-1} Mpc^{-1}, and $q_0 = 0.5$. We have reversed the calculation to recover the angular radius that corresponds to 16 kpc for galaxies in common to put their data on our curves.

TABLE 1

PHOTOMETRIC DATA FOR THE FIRST SEVERAL RANKED GALAXIES IN NEARBY CLUSTERS

Object	V_T	r''_e	$r''(\eta)$	$r''(\eta)$	$r''(\eta)$	$r''(\eta)$	$r''(\eta)$	$r''(\eta)$	$r''(\eta)$	$r''(\eta)$
z	$m - M$	R_e(kpc)	$V(\eta)$	$V(\eta)$	$V(\eta)$	$V(\eta)$	$V(\eta)$	$V(\eta)$	$V(\eta)$	$V(\eta)$
f	M_{V_T}	$\langle SB\rangle_e$	$\langle SB\rangle_{1.0}$	$\langle SB\rangle_{1.3}$	$\langle SB\rangle_{1.5}$	$\langle SB\rangle_{1.7}$	$\langle SB\rangle_{2.0}$	$\langle SB\rangle_{2.5}$	$\langle SB\rangle_{3.0}$	$\langle SB\rangle_{3.5}$
1	2	3	4	5	6	7	8	9	10	11
Leo N3379	9.3	48.2"	15.1"	47.9"	74.1"	93.3"	134.9"	257.0"	380.2"	
0.0025	30.88	3.5	10.8	10.0	9.8	9.6	9.5	9.3	9.3	
0.073	-21.6	19.7	18.0	19.7	20.4	20.7	21.4	22.6	23.4	
A42 G1*	14.9	13.6"	15.1"	21.9"	26.3"	31.6"	42.7"			
0.1087	39.07	43.0	15.6	15.3	15.2	15.1	15.1			
3.159	-24.1	22.6	22.8	23.3	23.6	23.9	24.5			
A85 G1*	12.7	33.1"	19.5"	31.6"	47.9"	66.1"	117.5"			
0.0499	37.38	48.1	13.9	13.5	13.3	13.1	12.9			
1.452	-24.7	22.3	21.5	22.2	22.9	23.5	24.5			
A85 G2	13.9	17.8"	4.8"	16.2"	24.5"	36.3"	50.1"			
0.0499	37.38	25.8	15.6	14.7	14.4	14.3	14.1			
1.452	-23.5	22.1	20.3	22.0	22.6	23.3	23.9			
A85 G3	14.8	4.5"	2.4"	4.7"	7.1"	11.0"	18.2"	27.5"		
0.0499	37.38	6.5	16.0	15.5	15.3	15.1	14.9	14.8		
1.452	-22.6	20.1	19.2	20.1	20.8	21.5	22.5	23.2		
A119 G1*	13.1	32.4"	13.5"	28.8"	41.7"	57.5"	83.2"			
0.0446	37.14	42.0	14.6	14.0	13.8	13.6	13.4			
1.297	-24.0	22.7	21.5	22.5	23.1	23.6	24.3			
A150 G1*	13.3	57.5"	9.3"	27.5"	53.7"	87.1"	166.0"			
0.0599	37.78	100.2	15.2	14.4	14.0	13.8	13.4			
1.742	-24.5	24.0	21.3	22.9	23.9	24.7	25.8			
A151 G1*	12.7	44.7"	15.8"	33.1"	64.6"	123.0"	263.0"			
0.0526	37.50	68.3	14.2	13.6	13.2	12.9	12.8			
1.530	-24.8	22.9	21.4	22.5	23.5	24.6	26.2			
A151 G2	14.6	5.8"	2.5"	6.3"	8.3"	13.2"	20.9"			
0.0526	37.50	8.9	16.0	15.3	15.1	14.9	14.7			
1.530	-22.9	20.4	19.2	20.5	21.0	21.7	22.6			
A194 N547*	11.5	47.9"	11.7"	23.4"	39.8"	63.1"	107.2"	199.5"	251.2"	
0.0178	35.14	24.8	13.2	12.7	12.4	12.1	11.9	11.8	11.7	
0.518	-23.6	21.9	19.8	20.8	21.6	22.4	23.3	24.5	25.0	
A194 N564	12.3	25.7"	10.7"	24.5"	38.0"	44.7"	75.9"	125.9"	141.3"	
0.0178	35.14	13.3	13.7	13.1	13.0	12.8	12.6	12.4	12.4	
0.518	-22.8	21.3	20.1	21.3	22.1	22.3	23.2	24.2	24.4	
A260 G1*	12.8	21.4"	6.0"	17.8"	38.0"	60.3"	128.8"			
0.0348	36.60	21.6	14.4	13.6	13.2	13.0	12.8			
1.012	-23.8	21.4	19.6	21.1	22.3	23.1	24.6			
A262 U1308+	10.7		12.3"	25.1"	316.2"	398.1"	416.9"			
0.0164	34.96		13.2	12.7	11.2	11.0	11.0			
0.477	-24.3		19.9	21.0	24.9	25.3	25.4			
A262 N708*	11.5	74.1"	18.6"	72.4"	95.5"	123.0"	169.8"	295.1"	389.0"	426.6"
0.0164	34.96	35.4	13.4	12.3	12.1	12.0	11.9	11.7	11.7	11.7"
0.477	-23.4	22.9	21.0	22.8	23.3	23.7	24.3	25.3	25.9	26.1"
A262 I171	12.1	24.0"	9.3"	18.6"	26.9"	38.0"	66.1"	120.2"	169.8"	
0.0164	34.96	11.4	13.6	13.1	12.8	12.6	12.4	12.3	12.2	
0.477	-22.8	21.0	19.6	20.6	21.2	21.8	22.8	23.9	24.6	
A262 N679	12.5	8.3"		12.9"	17.0"	29.5"	42.7"	69.2"	120.2"	138.0"
0.0164	34.96	4.0		13.3	13.2	13.1	12.7	12.6	12.5	12.5
0.477	-22.5	19.1		20.1	20.6	21.7	22.1	23.0	24.2	24.5
A262 N687	12.6	11.0"	3.1"	6.3"	14.8"	25.7"	36.3"	79.4"	123.0"	
0.0164	34.96	5.2	14.2	13.7	13.4	13.1	12.8	12.7	12.6	
0.477	-22.3	19.8	17.9	18.9	20.5	21.4	21.9	23.4	24.3	
A262 N759	12.9	8.1"				25.7"	36.3"	60.3"	79.4"	95.5"
0.0164	34.96	3.9				13.3	13.2	13.1	12.9	12.9
0.477	-22.1	19.4				21.6	22.2	23.2	23.7	24.0
A399 G1*	14.0	25.7"	19.5"	33.9"	38.9"	47.9"	57.5"			
0.0714	38.16	53.4	14.9	14.5	14.4	14.3	14.3			
2.077	-24.2	23.0	22.6	23.4	23.6	24.0	24.3			
A401 G1*	13.8		19.5"	39.8"	60.3"	83.2"	109.6"			
0.0746	38.25		14.9	14.4	14.1	14.0	13.9			
2.170	-24.5		22.6	23.6	24.3	24.8	25.3			
Perseus N1275+	11.2		9.1"	21.9"	39.8"	77.6"	169.8"	524.8"		
0.0183	35.20		12.9	12.3	11.9	11.6	11.3	10.9		
0.532	-24.0		19.0	20.2	21.2	22.3	23.7	25.8		
Perseus N1272+	11.7		6.3"	51.3"	64.6"	79.4"	100.0"	131.8"	169.8"	
0.0183	35.20		14.0	12.4	12.3	12.2	12.1	12.0	12.0	
0.532	-23.5		19.3	22.2	22.6	22.9	23.3	23.9	24.4	
Perseus N1278	12.6	15.8"	7.8"	16.6"	25.1"	33.1"	45.7"	54.3"	64.6"	81.3"
0.0183	35.20	8.4	13.9	13.4	13.0	12.9	12.8	12.8	12.7	12.7
0.532	-22.6	20.6	19.5	20.7	21.2	21.8	22.4	22.7	23.0	23.5
Perseus IC310	12.9	17.0"	4.9"	10.0"	20.4"	30.2"	49.0"	102.3"	162.2"	
0.0183	35.20	9.0	14.5	13.9	13.6	13.4	13.2	13.0	12.9	
0.532	-22.3	21.0	19.2	20.2	21.3	22.0	22.9	24.3	25.2	

TABLE 1—*Continued*

Object	V_T	r''_e	$r''(\eta)$	$r''(\eta)$	$r''(\eta)$	$r''(\eta)$	$r''(\eta)$	$r''(\eta)$	$r''(\eta)$	$r''(\eta)$
z	$m-M$	R_e(kpc)	$V(\eta)$	$V(\eta)$	$V(\eta)$	$V(\eta)$	$V(\eta)$	$V(\eta)$	$V(\eta)$	$V(\eta)$
f	M_{V_T}	$<SB>_e$	$<SB>_{1.0}$	$<SB>_{1.3}$	$<SB>_{1.5}$	$<SB>_{1.7}$	$<SB>_{2.0}$	$<SB>_{2.5}$	$<SB>_{3.0}$	$<SB>_{3.5}$
1	2	3	4	5	6	7	8	9	10	11
Perseus N1282	13.0	10.0"	4.8"	7.2"	12.6"	19.1"	31.6"	63.1"	74.1"	
0.0183	35.20	5.3	14.3	14.0	13.8	13.5	13.3	13.1	13.1	
0.532	-22.2	20.0	18.9	19.5	20.5	21.1	22.0	23.3	23.6	
Perseus N1293	13.0	15.1"	3.9"	7.9"	11.5"	16.2"	26.9"	56.2"	104.7"	
0.0183	35.20	8.0	14.6	14.1	14.0	13.8	13.5	13.3	13.2	
0.532	-22.2	20.9	18.8	19.9	20.6	21.1	21.9	23.3	24.6	
Perseus3/16.2	13.7	7.2"	3.4"	7.4"	10.2"	15.5"	20.4"	26.9"	36.3"	43.7"
0.0183	35.20	3.8	14.9	14.4	14.1	13.9	13.8	13.8	13.7	13.7
0.532	-21.5	20.0	18.8	19.9	20.4	21.1	21.6	22.1	22.8	23.1
Perseus N1283	13.9	10.0"	4.8"	6.5"	9.8"	16.6"	20.0"	50.1"	81.3"	
0.0183	35.20	5.3	15.1	14.9	14.7	14.4	14.3	14.0	14.0	
0.532	-21.3	20.9	19.8	20.2	20.9	21.7	22.0	23.7	24.8	
Perseus3/14.6	14.0	6.3"	1.1"	2.4"	4.9"	6.6"	11.0"	23.4"	36.3"	
0.0183	35.20	3.4	15.8	15.3	14.9	14.7	14.5	14.3	14.2	
0.532	-21.2	20.0	17.4	18.4	19.6	20.1	21.0	22.4	23.3	
Perseus N1273	13.1	8.9"	3.7"	6.8"	11.5"	17.0"	23.4"	38.0"	64.6"	83.2"
0.0183	35.20	4.7	14.5	14.0	13.8	13.6	13.5	13.4	13.2	13.1
0.532	-22.1	19.9	18.6	19.4	20.3	21.0	21.6	22.5	23.5	24.0
Perseus PER11	14.4	4.8"		6.0"	8.3"	10.5"	15.5"	21.4"	27.5"	38.0"
0.0183	35.20	2.6		15.0	15.0	14.9	14.8	14.7	14.6	14.5
0.532	-20.8	19.8		20.2	20.8	21.2	21.9	22.6	23.0	23.6
Perseus PER10	14.6	4.9"	2.5"	4.9"	6.2"	10.0"	18.6"	36.3"	57.5"	
0.0183	35.20	2.6	15.9	15.4	15.2	15.0	14.8	14.6	14.5	
0.532	-20.6	20.0	19.1	20.0	20.4	21.2	22.4	23.6	24.5	
A496 G1*	12.3	51.3"	26.3"	75.9"	89.1"	102.3"	162.2"			
0.0316	36.39	47.1	13.5	12.8	12.6	12.6	12.4			
0.919	-24.1	22.8	21.9	23.4	23.6	23.9	24.7			
A505 G1*	12.9	50.1"	12.6"	30.2"	45.7"	66.1"	97.7"	154.9"		
0.0540	37.55	78.7	14.6	14.0	13.7	13.6	13.4	13.2		
1.571	-24.6	23.4	21.4	22.6	23.3	23.9	24.6	25.4		
A514 G1*	14.8	8.9"	4.3"	8.3"	11.5"	15.8"	25.1"	33.1"		
0.0697	38.11	18.0	16.2	15.7	15.5	15.4	15.2	15.1		
2.027	-23.3	21.6	20.6	21.5	22.1	22.6	23.4	23.9		
A514 G3	15.1	10.5"	4.8"	7.8"	12.6"	17.0"				
0.0697	38.11	21.2	16.4	16.1	15.8	15.6				
2.027	-23.0	22.2	21.1	21.8	22.5	23.0				
A514 G2	15.5	8.7"	3.2"	5.6"		14.8"	30.2"			
0.0697	38.11	17.6	16.9	16.5		16.0	15.6			
2.027	-22.6	22.2	20.7	21.5		23.1	24.2			
A539 U3274*	12.3		19.5"	61.7"	114.8"	190.5"				
0.0267	36.02		14.2	13.3	12.9	12.5				
0.777	-23.7		21.9	23.5	24.5	25.1				
A539 ZW421	13.0	22.4"	4.8"	9.3"	19.1"	31.6"	63.1"	100.0"		
0.0267	36.02	17.4	14.7	14.3	13.9	13.6	13.3	13.2		
0.777	-23.0	21.7	19.4	20.4	21.5	22.3	23.6	24.4		
A539 G7	14.5	5.5"	5.1"	7.8"	9.1"	11.0"	14.5"	23.4"	33.1"	
0.0267	36.02	4.3	15.3	15.0	14.9	14.8	14.7	14.6	14.5	
0.777	-21.5	20.2	20.1	20.7	21.0	21.3	21.8	22.7	23.4	
A539 G4	14.2	10.5"	1.7"	4.6"	6.6"	10.7"	23.4"	53.7"	69.2"	
0.0267	36.02	8.2	15.9	15.4	15.2	14.9	14.6	14.4	14.4	
0.777	-21.8	21.3	18.3	19.9	20.5	21.3	22.7	24.3	24.8	
A539 G5	14.9	4.2"	1.4"	3.3"	6.5"	8.5"	12.3"	18.6"	39.8"	66.1"
0.0267	36.02	3.3	16.4	15.8	15.4	15.3	15.2	15.1	14.9	14.8
0.777	-21.2	19.9	18.4	19.6	20.7	21.2	21.9	22.7	24.1	25.2
A569 N2329*	12.2	22.9"	13.5"	26.3"	33.1"	41.7"	60.3"	104.7"	151.4"	
0.0193	35.32	12.9	13.4	12.9	12.7	12.6	12.5	12.3	12.2	
0.561	-23.1	21.0	20.3	21.2	21.6	21.9	22.6	23.6	24.4	
A569 U3696	12.8	16.2"	6.9"	12.6"	15.8"	20.0"	33.9"	83.2"	125.9"	
0.0193	35.32	9.1	14.1	13.7	13.6	13.5	13.2	13.0	12.9	
0.561	-22.5	20.9	19.6	20.5	20.8	21.2	22.1	23.8	24.6	
A569 G3	13.5	6.5"	7.4"	13.2"	20.9"	27.5"	36.3"	49.0"		
0.0193	35.32	3.6	14.1	13.8	13.6	13.5	13.4	13.3		
0.561	-21.9	19.5	19.7	20.6	21.4	21.9	22.4	23.0		
A569 G4	14.1	6.0"	7.9"	10.2"	12.0"	13.5"	16.6"	20.9"		
0.0193	35.32	3.4	14.6	14.3	14.3	14.2	14.2	14.1		
0.561	-21.3	19.9	20.3	20.6	20.9	21.1	21.5	21.9		
A569 G7	14.2	9.5"	4.6"	9.5"	13.2"	17.0"	25.1"	36.3"	42.7"	
0.0193	35.32	5.3	15.3	14.9	14.5	14.5	14.3	14.2	14.2	
0.561	-21.1	21.1	19.8	21.0	21.4	21.9	22.5	23.3	23.6	
A671 I2378*	13.0	30.9"	16.2"	36.3"	50.1"	60.3"	72.4"	83.2"	97.7"	
0.0497	37.37	44.7	14.3	13.6	13.4	13.3	13.3	13.2	13.2	
1.446	-24.4	22.4	21.5	22.7	23.2	23.5	23.8	24.1	24.4	

TABLE 1—*Continued*

Object	V_T	r''_e	$r''(\eta)$	$r''(\eta)$	$r''(\eta)$	$r''(\eta)$	$r''(\eta)$	$r''(\eta)$	$r''(\eta)$	$r''(\eta)$
z	$m - M$	R_e(kpc)	$V(\eta)$	$V(\eta)$	$V(\eta)$	$V(\eta)$	$V(\eta)$	$V(\eta)$	$V(\eta)$	$V(\eta)$
f	M_{V_T}	$<SB>_e$	$<SB>_{1.0}$	$<SB>_{1.3}$	$<SB>_{1.5}$	$<SB>_{1.7}$	$<SB>_{2.0}$	$<SB>_{2.5}$	$<SB>_{3.0}$	$<SB>_{3.5}$
1	2	3	4	5	6	7	8	9	10	11
A671 G2	14.0	11.7"	4.1"	11.0"	19.1"	25.1"	39.8"	67.6"	81.3"	
0.0497	37.37	16.9	15.5	14.7	14.4	14.3	14.1	14.0	13.9	
1.446	-23.4	21.3	19.8	21.2	22.1	22.5	23.4	24.4	24.7	
A671 G5	14.3	7.9"	3.7"	7.8"	10.7"	23.4"	30.9"	50.1"	60.3"	64.6"
0.0497	37.37	11.4	15.6	15.1	14.9	14.5	14.4	14.3	14.3	14.0
1.446	-23.1	20.8	19.7	20.8	21.3	22.6	23.1	24.1	24.4	24.3
A671 G3	14.6	7.2"	4.3"	8.3"	10.7"	14.5"	19.1"	25.7"	40.7"	60.3"
0.0497	37.37	10.4	15.7	15.2	15.1	14.9	14.8	14.8	14.7	14.6
1.446	-22.8	20.9	20.1	21.1	21.5	22.0	22.5	23.1	24.0	24.8
A671 G4	14.8	7.1"	2.3"	5.1"	8.5"	13.8"	24.0"	37.2"	49.0"	57.5"
0.0497	37.37	10.3	16.4	15.8	15.5	15.2	15.0	14.9	14.9	14.9
1.446	-22.5	21.1	19.5	20.6	21.4	22.2	23.2	24.0	24.5	24.9
A779 N2832*	11.6	30.9"	7.8"	33.9"	42.7"	60.3"	91.2"	147.9"	208.9"	
0.0223	35.63	20.0	13.4	12.4	12.2	12.0	11.9	11.7	11.7	
0.649	-24.0	21.1	19.1	21.2	21.6	22.2	22.9	23.8	24.5	
A957 U5515*	12.8		18.6"	41.7"	75.9"	93.3"				
0.0437	37.09		14.0	13.4	13.1	13.0				
1.271	-24.3		21.6	22.8	23.7	24.1				
A978 G1*	13.4	30.2"	9.8"	24.5"	38.0"	49.0"	72.4"	123.0"	173.8"	
0.0527	37.50	46.3	14.9	14.2	13.9	13.8	13.7	13.6	13.5	
1.533	-24.1	22.7	21.1	22.4	23.1	23.5	24.2	25.3	25.9	
A978 G2	15.1	6.3"	3.9"	7.4"	9.1"	12.3"	20.0"	22.9"	25.7"	31.6"
0.0527	37.50	9.7	16.1	15.7	15.6	15.4	15.3	15.2	15.2	15.2
1.533	-22.4	21.1	20.3	21.3	21.6	22.1	23.0	23.3	23.5	23.9
A978 G3	15.1	6.8"	4.7"	8.3"	11.5"	14.5"	19.1"	21.9"		
0.0527	37.50	10.4	16.2	15.7	15.5	15.4	15.4	15.3		
1.533	-22.4	21.3	20.8	21.6	22.1	22.5	23.0	23.3		
A978 G4	14.7	6.2"	1.9"	3.5"	6.3"	9.5"	15.8"	29.5"	51.3"	
0.0527	37.50	9.5	16.3	15.8	15.5	15.3	15.2	15.0	14.9	
1.533	-22.8	20.7	18.9	19.7	20.7	21.4	22.4	23.6	24.7	
A978 G5	15.6	3.2"	2.5"	6.3"	7.9"	9.5"	11.7"	14.8"	17.0"	24.5"
0.0527	37.50	4.9	16.5	15.9	15.7	15.7	15.6	15.5	15.5	15.5
1.533	-21.9	20.1	19.7	21.1	21.4	21.8	22.2	22.6	22.9	23.7
A993 G3*	13.9	16.3"	7.2"	10.7"	19.5"	28.8"	46.8"	64.6"	77.6"	
0.0533	37.52	25.3	15.2	14.9	14.5	14.4	14.2	14.1	14.0	
1.550	-23.6	22.0	20.7	21.3	22.2	22.9	23.8	24.4	24.7	
A993 G2	13.9	10.0"	4.9"	12.0"	15.1"	19.5"	32.4"	77.6"		
0.0533	37.52	15.5	15.3	14.8	14.6	14.4	14.2	14.0		
1.550	-23.6	20.9	20.0	21.4	21.7	22.1	23.0	24.7		
A993 G1	14.0	9.6"	6.5"	11.7"	19.5"	23.4"	30.9"	58.9"	79.4"	
0.0533	37.52	14.9	15.0	14.6	14.3	14.2	14.1	13.9	13.9	
1.550	-23.6	20.9	20.3	21.2	22.0	22.3	22.8	24.0	24.7	
A993 G5	14.2	24.5"	7.8"	10.2"	15.8"	24.5"	40.7"			
0.0533	37.52	38.0	15.6	15.4	15.3	15.0	14.8			
1.550	-23.3	23.1	21.3	21.7	22.5	23.2	24.1			
A994 G1*	13.6	10.2"	5.1"	9.8"	14.5"	20.0"	30.9"	42.7"	56.2"	63.1"
0.0390	36.85	11.6	14.8	14.4	14.1	14.0	13.8	13.7	13.7	13.7
1.134	-23.3	20.6	19.6	20.6	21.2	21.7	22.5	23.1	23.7	23.9
A1126 G1*	14.2	18.2"	12.6"	18.6"	24.5"	37.2"	52.5"	75.9"		
0.0828	38.48	43.8	15.2	14.9	14.7	14.5	14.4	14.3		
2.409	-24.3	22.4	21.9	22.5	22.9	23.6	24.2	24.9		
A1126 G2	15.5	10.7"	6.3"	16.6"	20.4"	24.5"				
0.0828	38.48	25.8	16.7	15.9	15.8	15.8				
2.409	-23.0	22.7	22.0	23.3	23.6	24.0				
A1139 U6057*	13.4	30.9"	8.1"	20.0"	30.9"	50.1"	75.9"	95.5"	117.5"	134.9"
0.0376	36.77	33.8	15.1	14.4	14.1	13.9	13.7	13.6	13.6	13.6
1.094	-23.4	22.8	20.9	22.1	22.8	23.6	24.4	24.8	25.2	25.5
A1139 G4	14.4	8.9"	4.3"	8.3"	10.5"	16.6"	21.4"	37.2"	51.3"	
0.0376	36.77	9.7	15.8	15.3	15.1	14.9	14.8	14.7	14.6	
1.094	-22.4	21.1	20.1	21.2	21.4	22.3	22.7	23.8	24.4	
A1139 G5	14.5	8.7"	4.4"	9.3"	12.0"	20.0"	30.2"	55.0"	67.6"	
0.0376	36.77	9.5	15.8	15.2	15.1	14.8	14.7	14.5	14.5	
1.094	-22.3	21.2	20.2	21.3	21.7	22.6	23.3	24.5	24.9	
A1139 G6	14.8	7.9"	2.2"	4.7"	7.9"	9.8"	19.1"	26.9"	44.7"	52.5
0.0376	36.77	8.6	16.3	15.8	15.6	15.3	15.1	14.9	14.9	14.8
1.094	-22.0	21.3	19.2	20.4	21.3	21.5	22.7	23.3	24.3	24.6
A1139 G7	14.6	9.1"	3.2"	7.8"	10.7"	15.8"	32.4"	64.6"	77.6"	
0.0376	36.77	10.0	16.1	15.5	15.3	15.1	14.9	14.7	14.6	
1.094	-22.1	21.4	19.9	21.2	21.7	22.4	23.7	24.9	25.3	
A1139 G3	14.3	9.8"	7.9"	12.3"	14.8"	20.4"	31.6"	47.9"	50.1"	55.0"
0.0376	36.77	10.7	15.2	14.9	14.8	14.6	14.5	14.3	14.3	14.3
1.094	-22.5	21.2	20.9	21.6	21.9	22.4	23.2	23.9	24.0	24.2

TABLE 1—*Continued*

Object	V_T	r''_e	$r''(\eta)$	$r''(\eta)$	$r''(\eta)$	$r''(\eta)$	$r''(\eta)$	$r''(\eta)$	$r''(\eta)$	$r''(\eta)$
z	$m-M$	R_e(kpc)	$V(\eta)$	$V(\eta)$	$V(\eta)$	$V(\eta)$	$V(\eta)$	$V(\eta)$	$V(\eta)$	$V(\eta)$
f	M_{V_T}	$\langle SB\rangle_e$	$\langle SB\rangle_{1.0}$	$\langle SB\rangle_{1.3}$	$\langle SB\rangle_{1.5}$	$\langle SB\rangle_{1.7}$	$\langle SB\rangle_{2.0}$	$\langle SB\rangle_{2.5}$	$\langle SB\rangle_{3.0}$	$\langle SB\rangle_{3.5}$
1	2	3	4	5	6	7	8	9	10	11
A1139 U6067	14.5	12.6"	8.3"	12.6"	16.6"	28.2"	38.9"	47.9"		
0.0376	36.77	13.8	15.5	15.2	15.1	14.8	14.7	14.6		
1.094	-22.3	22.0	21.4	22.0	22.4	23.3	23.9	24.3		
A1177 G1⋆	12.3	38.9"	8.3"	41.7"	75.9"	85.1"	100.0"	120.2"		
0.0319	36.41	36.1	14.3	13.0	12.6	12.6	12.5	12.5		
0.928	-24.1	22.2	20.1	22.3	23.3	23.5	23.7	24.1		
A1185 N3550⋆	12.8	15.8"	10.5"	15.8"	20.0"	30.2"	77.6"			
0.0349	36.60	16.0	14.0	13.8	13.7	13.5	13.1			
1.015	-23.8	20.8	20.3	21.0	21.5	22.1	23.8			
A1185 G7	13.9	7.8"	3.5"	9.3"	12.3"	16.6"	27.5"	40.7"	42.7"	
0.0349	36.60	7.9	15.3	14.6	14.4	14.3	14.1	14.0	14.0	
1.015	-22.7	20.4	19.2	20.7	21.1	21.6	22.5	23.3	23.4	
A1185 G8	14.5	8.5"	2.5"	6.3"	8.5"	11.0"	27.5"	72.4"		
0.0349	36.60	8.6	16.1	15.4	15.2	15.1	14.8	14.4		
1.015	-22.1	21.1	19.3	20.7	21.1	21.6	23.2	25.0		
A1185 N3558	13.5	14.8"	4.9"	10.7"	19.5"	32.4"	57.5"	81.3"	97.7"	107.2"
0.0349	36.60	15.0	15.1	14.5	14.1	13.9	13.7	13.6	13.5	13.5
1.015	-23.1	21.4	19.7	20.9	21.8	22.7	23.7	24.4	24.7	24.9
A1185 N3561	13.4	23.4"	12.0"	22.9"	30.2"	38.9"	51.3"	95.5"	104.7"	
0.0349	36.60	23.8	14.6	14.1	14.0	13.9	13.8	13.6	13.6	
1.015	-23.2	22.2	21.3	22.2	22.6	23.1	23.6	24.7	24.9	
A1190 G1⋆	14.6	15.1"	9.8"	20.4"	25.1"	32.4"	42.7"	63.1"		
0.0794	38.39	34.9	15.7	15.1	15.0	14.9	14.8	14.7		
2.310	-23.8	22.5	21.9	22.9	23.2	23.7	24.2	24.9		
A1190 G2	14.8	11.2"	4.0"	8.5"	18.6"	33.1"				
0.0794	38.39	25.9	16.3	15.7	15.3	15.0				
2.310	-23.6	22.0	20.6	21.6	22.9	23.9				
A1213 G1⋆	14.2	7.8"	3.5"	11.5"	14.8"	17.8"	25.7"			
0.0469	37.25	10.6	15.0	15.6	14.8	14.5	14.4	14.3		
1.364	-23.0	20.7	19.6	21.3	21.6	21.9	22.6			
A1213 G2	14.3	8.1"	6.5"	11.2"	13.5"	15.5"	20.0"	26.9"	51.3"	
0.0469	37.25	11.0	15.2	14.8	14.7	14.6	14.5	14.5	14.4	
1.364	-23.0	20.8	20.5	21.3	21.6	21.8	22.3	22.9	24.2	
A1213 G4	14.4	7.1"	2.3"	6.3"	11.2"	14.1"	20.0"	31.6"	47.9"	53.7"
0.0469	37.25	9.7	15.9	15.2	14.9	14.8	14.7	14.6	14.5	14.5
1.364	-22.8	20.7	19.0	20.5	21.4	21.8	22.4	23.3	24.2	24.4
A1213 G6	15.0	6.8"	6.3"	8.5"	10.0"	12.0"	16.2"	23.4"	25.7"	
0.0469	37.25	9.3	15.8	15.6	15.5	15.4	15.3	15.2	15.2	
1.364	-22.2	21.2	21.0	21.5	21.8	22.1	22.6	23.3	23.5	
A1228 U6394⋆	13.0	19.1"	8.3"	20.0"	30.9"	41.7"	56.2"	81.3"	104.7"	
0.0344	36.57	19.1	14.4	13.7	13.5	13.3	13.2	13.1	13.0	
1.001	-23.6	21.4	20.3	21.4	22.2	22.7	23.2	23.9	24.4	
A1228 I2744	13.6	17.4"	6.0"	11.7"	20.9"	31.6"	60.3"	77.6"		
0.0344	36.57	17.4	15.1	14.6	14.3	14.1	13.8	13.7		
1.001	-23.0	21.8	20.2	21.2	22.1	22.8	24.0	24.4		
A1228 I2738	13.7	9.8"	3.9"	7.2"	12.9"	19.1"	30.2"	45.7"	52.5"	79.4"
0.0344	36.57	9.8	15.1	14.5	14.3	14.1	13.9	13.8	13.8	13.7
1.001	-22.9	20.6	19.3	20.1	21.1	21.7	22.6	23.3	23.6	24.5
A1228 G4	14.0	9.5"	4.8"	10.5"	15.5"	17.0"	20.9"	38.9"	40.7"	50.1"
0.0344	36.57	9.5	15.3	14.7	14.5	14.4	14.4	14.2	14.2	14.1
1.001	-22.6	20.9	19.9	21.0	21.7	21.8	22.2	23.4	23.5	23.9
A1367 N3862⋆†	11.8	64.6"	9.1"	23.4"	120.2"	158.5"	204.2"	234.4"	288.4"	323.6"
0.0213	35.53	40.0	13.9	13.2	12.2	12.1	11.9	11.9	11.9	11.9
0.620	-23.8	22.8	19.9	21.3	23.8	24.3	24.7	25.0	25.4	25.6
A1367 N3842	11.9	33.1"	7.9"	24.5"	30.9"	60.3"	120.2"	204.2"	263.0"	269.2"
0.0213	35.53	20.5	13.6	12.8	12.7	12.4	12.1	11.9	11.9	11.9
0.620	-23.7	21.5	19.4	21.0	21.4	22.5	23.8	24.7	25.2	25.3
A1367 N3937	12.6	26.9"	9.3"	19.1"	25.7"	52.5"	72.4"	114.8"	138.0"	166.0
0.0213	35.53	16.7	14.1	13.6	13.4	13.0	12.9	12.8	12.7	12.7
0.620	-22.9	21.7	20.2	21.2	21.7	22.9	23.4	24.3	24.7	25.1
A1367 N3873	12.9	17.4"	4.1"	7.6"	12.3"	17.0"	33.1"	85.1"	109.6"	134.9"
0.0213	35.53	10.8	14.3	13.8	13.6	13.4	13.1	12.9	12.8	12.8
0.620	-22.6	21.1	18.6	19.5	20.3	20.8	22.0	23.7	24.2	24.7
A1367 N3910	12.8	13.5"	3.5"	8.5"	12.9"	18.6"	38.9"	64.6"	120.2"	131.8"
0.0213	35.53	8.4	14.5	13.9	13.6	13.4	13.2	13.0	12.9	12.9
0.620	-22.7	20.5	18.5	19.7	20.4	21.0	22.4	23.3	24.5	24.7
A1367 N3940	12.9	21.4"	8.3"	15.8"	21.4"	38.0"	51.3"	102.3"	151.4"	166.0"
0.0213	35.53	13.2	14.4	13.9	13.7	13.4	13.3	13.1	13.0	13.0
0.620	-22.6	21.6	20.2	21.1	21.6	22.6	23.1	24.4	25.2	25.4
A1367 N3886	12.9	10.7"	4.6"	9.1"	11.2"	16.2"	26.3"	40.7"	55.0"	79.4"
0.0213	35.53	6.6	14.4	13.8	13.7	13.6	13.3	13.1	13.1	13.0
0.620	-22.6	20.1	18.9	19.8	20.1	20.8	21.6	22.4	23.0	23.7

TABLE 1—*Continued*

Object	V_T	r''_e	$r''(\eta)$	$r''(\eta)$	$r''(\eta)$	$r''(\eta)$	$r''(\eta)$	$r''(\eta)$	$r''(\eta)$	$r''(\eta)$
z	$m - M$	R_e(kpc)	$V(\eta)$	$V(\eta)$	$V(\eta)$	$V(\eta)$	$V(\eta)$	$V(\eta)$	$V(\eta)$	$V(\eta)$
f	M_{V_T}	$\langle SB\rangle_e$	$\langle SB\rangle_{1.0}$	$\langle SB\rangle_{1.3}$	$\langle SB\rangle_{1.5}$	$\langle SB\rangle_{1.7}$	$\langle SB\rangle_{2.0}$	$\langle SB\rangle_{2.5}$	$\langle SB\rangle_{3.0}$	$\langle SB\rangle_{3.5}$
1	2	3	4	5	6	7	8	9	10	11
A1367 N3837	13.4	10.4"	6.3"	10.0"	12.6"	16.6"	21.9"	40.7"	58.9"	
0.0213	35.53	6.4	14.5	14.2	14.0	13.9	13.8	13.6	13.5	
0.620	-22.2	20.5	19.7	20.4	20.8	21.2	21.7	22.9	23.6	
A1691 G1*	13.6	30.2"	10.2"	19.1"	31.6"	47.9"	57.5"			
0.0722	38.18	63.4	15.2	14.6	14.3	14.1	14.0			
2.100	-24.6	23.0	21.5	22.3	23.1	23.8	24.1			
A1767 G1*	14.1	16.6"		20.9"	31.6"	36.3"				
0.0756	38.28	36.5		14.6	14.4	14.3				
2.199	-24.2	22.2		22.5	23.1	23.4				
A1785 G1*	14.9	12.0"	1.5"	2.3"	3.2"	12.0"	30.9"			
0.0792	38.38	27.7	16.8	16.5	16.3	15.7	15.3			
2.304	-23.5	22.3	19.0	19.6	20.1	22.3	24.0			
A1809 G1*	13.9	30.2"	3.7"	9.5"	32.4"	52.5"	107.2"			
0.0788	38.37	69.3	15.9	15.2	14.5	14.2	13.9			
2.292	-24.5	23.3	20.0	21.4	23.3	24.1	25.3			
A1809 G2	15.4	7.9"	3.0"	5.0"	9.1"	17.8"	30.9"			
0.0788	38.37	18.2	16.8	16.5	16.1	15.8	15.6			
2.292	-22.9	21.9	20.5	21.2	22.2	23.3	24.3			
A1809 G3	16.1	3.4"	2.6"	4.4"	5.2"	6.6"	9.5"	16.6"		
0.0788	38.37	7.8	17.1	16.7	16.6	16.5	16.3	16.2		
2.292	-22.3	20.7	20.4	21.1	21.4	21.8	22.5	23.5		
A1904 G1*	13.6	20.4"	5.4"	26.3"	45.7"	51.3"	66.1"			
0.0714	38.16	42.4	15.4	14.2	13.9	13.8	13.7			
2.077	-24.5	22.2	20.3	22.6	23.4	23.6	24.1			
A1913 G1*	13.9	25.7"	4.3"	7.2"	25.7"	51.3"	79.4"			
0.0533	37.52	39.9	15.8	15.4	14.7	14.3	14.2			
1.550	-23.6	23.0	20.2	21.0	23.0	24.1	25.0			
A1913 G5	14.7	7.6"	2.6"	4.8"	7.1"	9.5"	17.0"	32.4"	58.9"	
0.0533	37.52	11.8	16.2	15.7	15.5	15.4	15.1	15.0	14.9	
1.550	-22.8	21.1	19.6	20.4	21.0	21.5	22.5	23.8	25.0	
A1913 G4	14.8	5.8"	3.1"	5.0"	6.5"	10.0"	13.2"	26.3"	30.2"	
0.0533	37.52	8.9	16.0	15.6	15.5	15.3	15.2	15.0	14.9	
1.550	-22.7	20.6	19.7	20.4	20.8	21.5	22.0	23.3	23.6	
A1913 G2	14.9	3.5"	2.6"	3.9"	5.0"	7.6"	10.7"	24.0"		
0.0533	37.52	5.4	16.0	15.7	15.5	15.3	15.2	15.0		
1.550	-22.6	19.7	19.3	19.9	20.3	21.0	21.6	23.1		
A1913 G3	14.9	7.1"	7.4"	9.1"	11.5"	15.1"	18.6"	26.9"	37.2"	
0.0533	37.52	11.0	15.6	15.4	15.3	15.2	15.1	15.0	15.0	
1.550	-22.6	21.1	21.2	21.5	21.9	22.3	22.7	23.4	24.1	
A1913 G7	15.2	5.2"	2.6"	4.0"	7.1"	13.2"	19.1"			
0.0533	37.52	8.1	16.4	16.2	15.9	15.5	15.4			
1.550	-22.3	20.8	19.7	20.4	21.4	22.3	23.0			
A1983 G6	14.0	11.0"	5.1"	9.1"	11.7"	15.8"	31.6"	50.1"		
0.0458	37.20	14.6	15.0	14.8	14.7	14.5	14.1	14.0		
1.332	-23.2	21.2	19.8	20.8	21.3	21.7	22.8	23.7		
A1983 G2	14.2	6.3"	2.9"	5.5"	9.1"	13.5"	22.4"	50.1"	63.1"	
0.0458	37.20	8.4	15.5	15.0	14.7	14.5	14.3	14.1	14.0	
1.332	-23.0	20.2	19.0	19.9	20.7	21.4	22.3	23.8	24.3	
A1983 G8	14.3	7.4"	3.3"	9.1"	10.5"	13.2"	19.1"	38.0"	63.1"	
0.0458	37.20	9.9	15.7	14.9	14.9	14.8	14.7	14.6	14.4	
1.332	-22.8	20.6	19.5	20.9	21.2	21.6	22.3	23.7	24.6	
A1983 G7	14.4	5.0"	5.0"	8.3"	10.0"	12.3"	14.1"	24.0"	28.2"	30.9"
0.0458	37.20	6.7	15.2	14.8	14.7	14.6	14.6	14.5	14.4	14.4
1.332	-22.8	19.9	19.9	20.7	21.0	21.3	21.6	22.6	22.9	23.1
A1983 G3	14.6	10.0"	5.0"	12.9"	16.6"	19.5"	25.7"			
0.0458	37.20	13.3	15.9	15.2	15.0	14.9	14.8			
1.332	-22.6	21.6	20.6	22.0	22.4	22.6	23.1			
A1991 G1*	13.3	37.2"	19.1"	31.6"	42.7"	61.7"	75.9"			
0.0589	37.74	63.7	14.5	14.1	14.0	13.8	13.7			
1.713	-24.4	23.2	22.2	22.9	23.4	24.0	24.4			
A2028 G1*	14.3		3.8"	25.1"						
0.0772	38.33		16.1	14.7						
2.246	-24.0		20.2	22.9						
A2029 G1*+	12.9	41.7"	16.6"	38.9"	57.5"	74.1"	104.7"	166.0"		
0.0767	38.32	93.0	14.3	13.6	13.4	13.3	13.2	13.1		
2.231	-25.4	23.0	21.7	22.8	23.5	23.9	24.5	25.4		
A2052 G1*	12.5	40.0"	26.9"	61.7"	85.1"	97.7"	112.2"	154.9"		
0.0348	36.60	40.5	13.6	13.0	12.8	12.7	12.7	12.6		
1.012	-24.1	22.5	22.0	23.2	23.7	23.9	24.2	24.8		
A2061 G1*	14.0	19.5"	4.4"	8.1"	37.2"	46.8"	63.1"	77.6"		
0.0768	38.32	43.6	15.8	15.3	14.4	14.3	14.2	14.1		
2.234	-24.3	22.5	20.2	21.1	23.5	23.9	24.4	24.8		

TABLE 1—*Continued*

Object z f 1	V_T $m-M$ M_{V_T} 2	r''_e R_e(kpc) $\langle SB\rangle_e$ 3	$r''(\eta)$ $V(\eta)$ $\langle SB\rangle_{1.0}$ 4	$r''(\eta)$ $V(\eta)$ $\langle SB\rangle_{1.3}$ 5	$r''(\eta)$ $V(\eta)$ $\langle SB\rangle_{1.5}$ 6	$r''(\eta)$ $V(\eta)$ $\langle SB\rangle_{1.7}$ 7	$r''(\eta)$ $V(\eta)$ $\langle SB\rangle_{2.0}$ 8	$r''(\eta)$ $V(\eta)$ $\langle SB\rangle_{2.5}$ 9	$r''(\eta)$ $V(\eta)$ $\langle SB\rangle_{3.0}$ 10	$r''(\eta)$ $V(\eta)$ $\langle SB\rangle_{3.5}$ 11
A2061 G3	14.6	14.3"	4.0"	7.9"	12.0"	40.7"				
0.0768	38.32	31.9	16.2	15.7	15.4	14.8				
2.234	-23.7	22.3	20.4	21.4	22.0	24.1				
A2061 G2	15.0	7.2"	4.1"	7.6"	9.3"	12.9"	25.1"			
0.0768	38.32	16.2	16.1	15.7	15.6	15.4	15.2			
2.234	-23.3	21.3	20.4	21.3	21.7	22.2	23.4			
A2063 G1*	13.0	25.1"	18.6"	30.9"	38.9"	47.9"	58.9"			
0.0337	36.53	24.6	14.0	13.6	13.5	13.4	13.3			
0.980	-23.5	22.0	21.6	22.3	22.7	23.0	23.4			
A2063 G2	14.4	8.1"	2.9"	6.3"	7.6"	8.9"	24.5"	28.8"		
0.0337	36.53	8.0	15.9	15.3	15.2	15.1	16.7	14.6		
0.980	-22.1	20.9	19.4	20.5	20.8	21.1	24.9	23.2		
A2063 G3	15.0	4.3"	3.1"	5.1"	6.8"	8.3"	11.0"	15.8"	23.4"	
0.0337	36.53	4.2	16.0	15.6	15.5	15.4	15.3	15.2	15.1	
0.980	-21.5	20.2	19.7	20.4	20.9	21.2	21.7	22.4	23.2	
A2065 G1*	13.8	38.0"	17.0"	49.0"	66.1"	81.3"	100.0"	120.2"		
0.0721	38.18	79.7	15.3	14.5	14.3	14.2	14.0	14.0		
2.097	-24.3	23.7	22.7	24.2	24.7	25.0	25.3	25.6		
A2065 G2	14.4	30.2"	11.2"	19.1"	30.9"	63.1"	102.3"	162.2"	166.0"	
0.0721	38.18	63.3	15.8	15.4	15.1	14.8	14.7	14.6	14.6	
2.097	-23.8	23.8	22.3	23.1	23.8	25.1	26.0	26.9	26.9	
A2107 G1*	12.8	28.2"	14.5"	32.4"	46.8"	63.1"	81.3"	141.3"	158.5"	169.8"
0.0425	37.03	34.8	14.1	13.5	13.3	13.1	13.0	12.9	12.9	12.9
1.236	-24.2	22.1	21.1	22.3	22.9	23.4	23.8	24.9	25.1	25.3
A2124 G1*	13.8	18.2"	16.2"	26.9"	32.4"	38.9"	42.7"	55.0"	63.1"	79.4"
0.0669	38.02	35.4	14.6	14.2	14.1	14.0	14.0	13.9	13.9	13.9
1.946	-24.3	22.0	21.9	22.6	22.9	23.2	23.4	23.9	24.1	24.6
A2147 G1*	12.1		13.2"	24.5"						
0.0357	36.65		14.3	13.8						
1.038	-24.6		21.1	22.0						
A2151 N6034+	12.2		8.5"	19.1"	33.1"	120.2"				
0.0371	36.74		14.7	14.1	13.8	13.1				
1.079	-24.6		20.6	21.8	22.6	24.8				
A2151 N6047*	13.1	31.6"	6.0"	12.3"	24.0"	31.6"	40.7"	55.0"	120.2"	
0.0371	36.74	34.1	14.9	14.4	14.0	13.8	13.6	13.5	13.3	
1.079	-23.7	22.6	20.1	21.0	22.1	22.5	22.9	23.4	24.9	
A2151 N6055	13.6	15.8"	4.4"	8.7"	13.5"	29.5"	52.5"	81.3"	97.7"	
0.0371	36.74	17.1	15.4	14.7	14.4	14.0	13.8	13.7	13.7	
1.079	-23.2	21.6	19.8	20.6	21.3	22.6	23.7	24.5	24.9	
A2151 N6061	13.6	8.7"	3.7"	7.6"	12.9"	24.0"	30.9"	52.5"	75.9"	93.3"
0.0371	36.74	9.4	15.0	14.5	14.2	13.9	13.8	13.7	13.6	13.6
1.079	-23.1	20.3	19.1	20.1	21.0	22.1	22.5	23.5	24.3	24.7
A2151 N6057	14.2	19.1"	3.5"	6.3"	10.7"	15.1"	19.5"	33.9"	50.1"	
0.0371	36.74	20.6	16.0	15.6	15.1	15.0	14.9	14.8	14.7	
1.079	-22.6	22.6	20.0	20.8	21.5	22.1	22.6	23.7	24.4	
A2152 G1*	14.0	5.0"	4.0"	5.0"	6.3"	9.5"	20.0"	38.9"	52.5"	
0.0383	36.81	5.6	15.1	15.0	14.8	14.6	14.2	14.2	14.1	
1.114	-22.8	19.5	19.3	19.7	20.1	20.7	22.0	23.4	23.9	
A2152 G2	14.2	12.8"		7.9"	12.9"	18.6"	29.5"	50.1"	77.6"	97.7"
0.0383	36.81	14.3		15.2	15.0	14.8	14.6	14.4	14.3	14.3
1.114	-22.6	21.8		20.9	21.8	22.3	23.2	24.1	25.0	25.5
A2152 G3	14.3	8.5"	4.2"	6.8"	9.8"	19.1"	26.3"	31.6"	39.8"	46.8"
0.0383	36.81	9.5	15.5	15.1	15.0	14.6	14.5	14.5	14.4	14.4
1.114	-22.5	20.9	19.8	20.5	21.2	22.3	22.9	23.2	23.7	24.0
A2162 G1+	11.7		4.8"	13.5"	199.5"	251.2"	309.0"			
0.0318	36.40		14.7	13.9	12.2	12.1	11.9			
0.925	-24.7		19.4	20.8	24.9	25.3	25.6			
A2197 N6173*+	11.4	95.5"	26.3"	40.7"	154.9"	251.2"	331.1"	371.5"	489.8"	
0.0303	36.30	84.2	13.1	12.7	11.9	11.7	11.6	11.5	11.5	
0.881	-24.9	23.3	21.4	22.0	24.1	24.9	25.4	25.6	26.2	
A2197 N6160	12.2	41.7"	18.2"	50.1"	66.1"	77.6"	95.5"	144.5"	154.9"	166.0"
0.0303	36.30	36.7	13.6	12.8	12.7	12.6	12.5	12.4	12.4	12.4
0.881	-24.1	22.3	21.2	22.6	23.0	23.3	23.6	24.4	24.6	24.7
A2197 N6146	12.7	21.9"	20.0"	28.8"	33.1"	49.0"	66.1"	93.3"		
0.0303	36.30	19.3	13.5	13.2	13.1	13.0	12.8	12.7		
0.881	-23.6	21.4	21.3	21.8	22.0	22.7	23.2	23.8		
A2199 N6166*+	11.3	102.3"	17.0"	28.2"	52.5"	331.1"	398.1"	446.7"	512.9"	
0.0305	36.31	90.8	13.2	12.8	12.5	11.5	11.4	11.4	11.4	
0.887	-25.0	23.4	20.6	21.3	22.3	25.4	25.7	25.9	26.2	
A2255 G1*	14.0	20.4"	10.2"	25.1"	31.6"	41.7"	58.9"			
0.0769	38.32	45.7	15.3	14.6	14.5	14.4	14.3			
2.237	-24.3	22.6	21.6	22.9	23.2	23.7	24.4			

TABLE 1—*Continued*

Object	V_T	r''_e	$r''(\eta)$	$r''(\eta)$	$r''(\eta)$	$r''(\eta)$	$r''(\eta)$	$r''(\eta)$	$r''(\eta)$	$r''(\eta)$
z	$m-M$	R_e(kpc)	$V(\eta)$	$V(\eta)$	$V(\eta)$	$V(\eta)$	$V(\eta)$	$V(\eta)$	$V(\eta)$	$V(\eta)$
f	M_{V_T}	$\langle SB\rangle_e$	$\langle SB\rangle_{1.0}$	$\langle SB\rangle_{1.3}$	$\langle SB\rangle_{1.5}$	$\langle SB\rangle_{1.7}$	$\langle SB\rangle_{2.0}$	$\langle SB\rangle_{2.5}$	$\langle SB\rangle_{3.0}$	$\langle SB\rangle_{3.5}$
1	2	3	4	5	6	7	8	9	10	11
A2255 G2+	14.2	20.0"	3.0"	22.4"	28.8"					
0.0769	38.32	44.7	16.5	14.9	14.7					
2.237	-24.1	22.7	20.1	22.9	23.3					
A2255 G3	14.8	10.2"	4.7"	13.5"	20.9"	24.5"				
0.0769	38.32	22.9	16.1	15.3	15.1	15.0				
2.237	-23.6	21.8	20.7	22.2	22.9	23.2				
A2256 G1*	13.4	17.8"	12.3"	23.4"	38.9"	49.0"	67.6"			
0.0601	37.79	31.1	14.5	14.0	13.7	13.6	13.6			
1.748	-24.3	21.7	21.2	22.1	22.9	23.3	23.9			
A2256 U1072	13.9	8.9"	6.0"	9.3"	12.0"	23.4"				
0.0601	37.79	15.6	15.0	14.6	14.5	14.2				
1.748	-23.9	20.7	20.1	20.7	21.1	22.3				
A2256 G4	14.7	6.2"	3.3"	5.9"	9.5"	12.9"	18.6"			
0.0601	37.79	10.8	15.9	15.4	15.2	15.0	14.9			
1.748	-23.1	20.6	19.7	20.5	21.3	21.8	22.5			
A2366 G1*	13.4	27.5"	4.3"	8.3"	30.2"	37.2"	95.5"			
0.0542	37.56	43.4	15.4	14.9	14.1	14.0	13.6			
1.577	-24.2	22.6	19.8	20.7	22.7	23.1	24.8			
A2400 G1*	14.9	12.9"	5.9"	13.2"	18.6"	24.0"	32.4"			
0.0881	38.62	33.0	16.2	15.6	15.4	15.3	15.2			
2.563	-23.8	22.4	21.3	22.4	23.0	23.4	24.0			
A2400 G2	15.3	6.8"	3.2"	5.8"	11.2"	17.0"	21.9"	27.5"		
0.0881	38.62	17.4	16.6	16.1	15.7	15.5	15.4	15.4		
2.563	-23.3	21.4	20.3	21.2	22.2	22.9	23.4	23.8		
A2420 G1*	14.1	24.5"	9.5"	39.8"						
0.0823	38.47	58.7	15.6	14.5						
2.394	-24.3	23.1	21.7	23.8						
A2420 G2	15.9	4.1"	3.4"	5.2"	7.4"					
0.0823	38.47	9.8	16.9	16.4	16.1					
2.394	-22.5	21.0	20.8	21.3	21.7					
A2440 G1*	14.9	15.8"	7.1"	10.7"	13.8"	20.9"	26.9"			
0.0904	38.67	41.6	16.2	16.1	15.8	15.5	15.4			
2.630	-23.8	22.9	21.7	22.5	22.8	23.3	23.8			
A2440 G2	15.2	12.6"	5.2"	15.8"	30.2"	45.7"				
0.0904	38.67	33.1	16.7	15.8	15.4	15.3				
2.630	-23.5	22.7	21.5	23.1	24.1	24.9				
A2440 G3	15.7	5.8"	2.6"	4.7"	6.3"	8.3"	16.6"			
0.0904	38.67	15.2	17.0	16.6	16.4	16.2	16.0			
2.630	-23.0	21.5	20.3	21.2	21.6	22.1	23.3			
A2457 G1*	13.9	19.1"	7.9"	15.5"	25.7"	39.8"	63.1"			
0.0595	37.76	33.0	15.3	14.8	14.5	14.3	14.1			
1.731	-23.9	22.3	21.0	22.0	22.8	23.5	24.4			
A2469 G1*+	15.4	6.5"	6.0"	7.9"	10.0"	12.6"	17.8"			
0.0656	37.98	12.4	16.2	16.0	15.8	15.7	15.6			
1.908	-22.6	21.4	21.4	21.7	22.1	22.5	23.1			
A2589 G1+*	12.4	81.3"	15.8"	66.1"	104.7"	120.2"	125.9"			
0.0420	37.01	99.3	14.4	13.3	13.0	13.0	12.9			
1.222	-24.6	23.9	21.6	23.6	24.4	24.6	24.7			
A2634 G1+*	12.2	51.1"	5.0"	24.5"	50.1"	77.6"	169.8"	208.9"		
0.0322	36.43	47.8	14.6	13.4	12.9	12.7	12.4	12.3		
0.937	-24.3	22.7	19.4	21.6	22.7	23.4	24.8	25.1		
A2634 N7728	12.5	20.0"	5.9"	10.0"	15.1"	20.0"	30.2"	114.8"	131.8"	
0.0322	36.43	18.7	14.0	13.6	13.4	13.3	13.1	12.6	12.6	
0.937	-23.9	21.0	19.1	19.8	20.5	21.0	21.7	24.2	24.4	
A2634 U12744	12.9	18.2"	7.4"	14.5"	25.1"	32.4"	50.1"	85.1"	100.0"	120.2"
0.0322	36.43	17.0	14.3	13.8	13.5	13.4	13.2	13.1	13.0	13.0
0.937	-23.5	21.2	19.9	20.9	21.8	22.2	22.9	24.0	24.3	24.7
A2634 U12733	13.3	9.1"	2.8"	5.2"	10.5"	15.5"	24.0"	50.1"		
0.0322	36.43	8.5	14.9	14.4	13.9	13.8	13.6	13.4		
0.937	-23.1	20.1	18.3	19.3	20.2	20.9	21.7	23.1		
A2666 N7768*	12.0	30.9"	12.0"	15.5"	25.1"	38.9"	102.3"	162.2"	199.5"	234.4"
0.0273	36.07	24.5	13.3	13.1	12.9	12.6	12.3	12.1	12.1	12.1
0.794	-24.1	21.4	19.9	20.3	21.1	21.8	23.6	24.4	24.8	25.2
A2670 G1+	12.8	190.5"	4.2"	9.8"	22.4"					
0.0749	38.26	415.2	15.8	15.1	14.6					
2.179	-25.5	26.1	20.1	21.3	22.6					
A2700 G1*	14.5	15.8"	13.2"	20.0"	28.2"	34.7"	51.3"			
0.0978	38.84	45.0	15.4	15.1	14.9	14.8	14.6			
2.845	-24.3	22.5	22.3	22.8	23.4	23.7	24.4			
DC107 G2*	12.0	32.4"	14.8"	31.6"	40.7"	52.5"	79.4"	141.3"		
0.0229	35.70	21.6	13.3	12.8	12.6	12.5	12.4	12.2		
0.666	-23.7	21.5	20.4	21.5	21.9	22.3	23.1	24.2		

TABLE 1—*Continued*

Object z f 1	V_T $m-M$ M_{V_T} 2	r''_e R_e(kpc) $\langle SB \rangle_e$ 3	$r''(\eta)$ $V(\eta)$ $\langle SB \rangle_{1.0}$ 4	$r''(\eta)$ $V(\eta)$ $\langle SB \rangle_{1.3}$ 5	$r''(\eta)$ $V(\eta)$ $\langle SB \rangle_{1.5}$ 6	$r''(\eta)$ $V(\eta)$ $\langle SB \rangle_{1.7}$ 7	$r''(\eta)$ $V(\eta)$ $\langle SB \rangle_{2.0}$ 8	$r''(\eta)$ $V(\eta)$ $\langle SB \rangle_{2.5}$ 9	$r''(\eta)$ $V(\eta)$ $\langle SB \rangle_{3.0}$ 10	$r''(\eta)$ $V(\eta)$ $\langle SB \rangle_{3.5}$ 11
AWM1 G1*	12.6	25.7"	6.6"	19.5"	31.6"	42.7"	69.2"	134.9"	186.2"	204.2"
0.0265	36.01	19.8	14.2	13.5	13.3	13.1	12.9	12.7	12.7	12.7
0.771	-23.4	21.6	19.5	21.2	22.0	22.5	23.4	24.6	25.3	25.5
AWM2 N4213*	12.6	24.5"	5.0"	11.0"	39.8"	58.9"	67.6"	93.3"	100.0"	123.0"
0.0223	35.63	15.9	14.5	13.9	13.2	13.0	12.9	12.8	12.8	12.8
0.649	-23.0	21.6	19.2	20.3	22.4	23.0	23.3	23.9	24.0	24.5
AWM3 N5629*	11.5	83.2"	5.4"	16.6"	24.0"	49.0"	104.7"			
0.0152	34.80	36.8	13.9	13.1	12.9	12.6	12.3			
0.442	-23.3	23.1	18.8	20.4	21.0	22.2	23.6			
AWM4 N6051*	12.7	28.8"	16.2"	33.9"	47.9"	58.9"	95.5"	144.5"	162.2"	
0.0307	36.33	25.8	13.9	13.3	13.1	13.0	12.9	12.8	12.7	
0.893	-23.7	22.0	21.2	22.2	22.8	23.1	24.0	24.8	25.0	
AWM5 N6269*	12.2	37.2"	6.8"	22.4"	45.7"	70.8"	102.3"	166.0"	199.5"	
0.0342	36.56	37.0	14.0	13.2	12.8	12.6	12.4	12.3	12.3	
0.995	-24.4	22.0	19.4	21.2	22.4	23.1	23.7	24.7	25.0	
AWM6 G1*	12.6	32.4"	9.3"	33.9"	46.8"	63.1"	89.1"	123.0"	128.8"	
0.0357	36.65	33.6	14.2	13.3	13.1	12.9	12.8	12.7	12.7	
1.038	-24.1	22.1	20.3	22.2	22.7	23.2	23.8	24.4	24.5	
MKW2 G1*	12.7	27.5"	8.3"	19.5"	50.1"	60.3"	91.2"	128.8"		
0.0291	36.21	23.3	14.2	13.7	13.1	13.0	12.9	12.8		
0.846	-23.5	21.9	20.1	21.4	22.9	23.2	23.9	24.6		
MKW4 N4073*	11.2	52.5"	26.9"	52.5"	79.4"	97.7"	134.9"	177.8"	234.4"	263.0"
0.0186	35.24	28.4	12.4	12.0	11.8	11.6	11.5	11.4	11.3	11.3
0.541	-24.1	21.8	20.8	21.8	22.5	22.8	23.4	23.8	24.4	24.6
MKW5 N5400*	12.8	21.9"	11.0"	23.4"	32.4"	49.0"	64.6"	85.1"	97.7"	
0.0238	35.77	15.1	13.9	13.4	13.2	13.1	13.0	12.9	12.9	
0.692	-23.0	21.4	20.4	21.5	22.0	22.8	23.3	23.8	24.0	
MKW9 G1*	13.3	25.7"	18.6"	30.2"	50.1"	64.6"	81.3"	100.0"	123.0"	131.8"
0.0376	36.77	28.1	14.4	14.0	13.7	13.6	13.5	13.4	13.4	13.4
1.094	-23.4	22.4	21.9	22.6	23.5	23.9	24.3	24.7	25.1	25.3

cluster name, where applicable, or by the designation given by Schombert (1987). Note again that the listed magnitudes are on the V system, differing from the data in SPII which we used on the B system.

The entries in Table 1 are as follows:

The three entries in column (1) for each galaxy give the galaxy name, the redshift, and the factor f by which to multiply the angular radius to calculate the linear radius in kiloparsecs. The f factor is derived from the redshift and an assumed Hubble constant of 50 km s^{-1} Mpc^{-1}. The adopted redshifts are from Schombert's summary. The first-ranked galaxy in a given cluster has an asterisk suffixed to the name. CD galaxies or galaxies with companions that may distort the luminosity profile have a Greek cross suffixed to the name.

The three entries in column (2) are (*a*) the "total" V magnitude read from our calculated and corrected $m(\infty)$ growth curve, (*b*) the adopted distance modulus found from the redshift using $H_0 = 50$ km s^{-1} Mpc^{-1}, and (*c*) the absolute V "total" magnitude found by combining the first two entries.

Column (3) gives (*a*) the measured angular "effective" radius in arcseconds found from the $m(r)$ growth curve read for the r value at $V_T + 0.75$, (*b*) the resulting linear radius obtained by multiplying r''_e by f, and (*c*) the average "effective" surface brightness found by combining $V_T + 0.75$ and r_e; the units are V mag $arcsec^{-2}$.

Columns (4)–(11) give data read at Petrosian η values of 1.0, 1.3, 1.5, 1.7, 2.0, 2.5, 3.0, and 3.5. Shown in the three rows for each galaxy are (*a*) the η radius in arcseconds, (*b*) the apparent V magnitude enclosed within that radius as obtained from the corrected $m(r)$ growth curve, and (*c*) the resulting $SB_{V(\eta)}$ averaged over that radius.

3. CORRELATIONS BETWEEN LINEAR RADII, ABSOLUTE LUMINOSITY, AND AVERAGE SURFACE BRIGHTNESS FOR THE SEVERAL BRIGHTEST CLUSTER GALAXIES

In the correlations between linear radii, $\langle SB \rangle$, and M we make the distinction between the first-ranked galaxy in a given cluster and the fainter members of the same cluster. When data for the entire sample are shown, different symbols separate the first-ranked galaxies from those of lower rank in the diagrams.

3.1. *Variation of R with Absolute Magnitude*

Consider first the variation of linear radius with absolute magnitude for E galaxies discussed in SPII (Figs. 4–7). It was shown there that Hubble's (1926) constant surface brightness scaling law of $M \sim -5 \log R$ applies only over the very restricted range of absolute magnitude of $-22 < M(V)_T < -19$. We continue that discussion here using the present sample to extend the correlation between R and M beyond the parameter range studied in SPII.

Figure 1 shows the data from Table 1. First-ranked galaxies are solid dots; non–first-ranked are open circles. Lines of constant $\langle SB \rangle$ are the solid lines. Data for four Petrosian η-values are shown. Radii increase faster with increasing luminosity than dex $0.2M$, giving progressively fainter $\langle SB \rangle$ as M becomes brighter. This behavior is similar to that in SPII but is now extended to brighter magnitudes, as shown in Figure 2

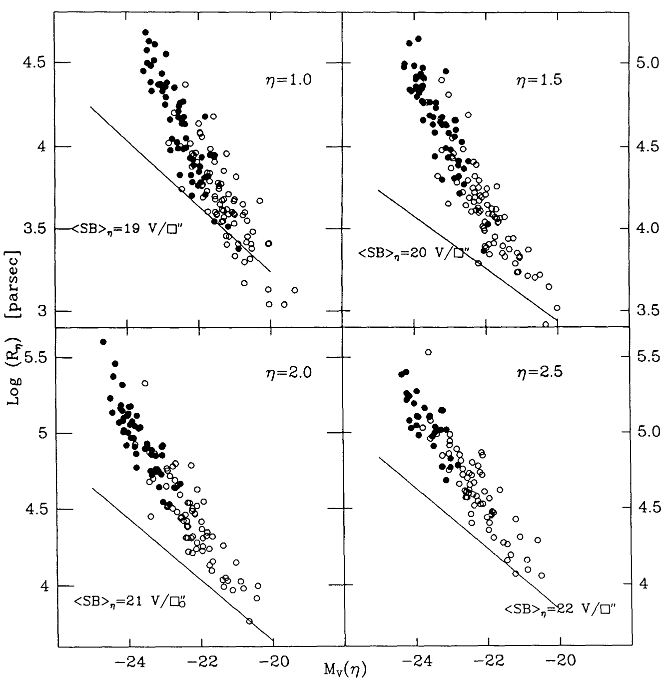

FIG. 1.—Variation of Petrosian linear radii with absolute V magnitude for the total sample in Table 1. Closed and open circles are first-ranked and non–first-ranked galaxies, respectively. Lines of constant surface brightness are shown. The linear radii are calculated using $H_0 = 50$ km s^{-1} Mpc^{-1}.

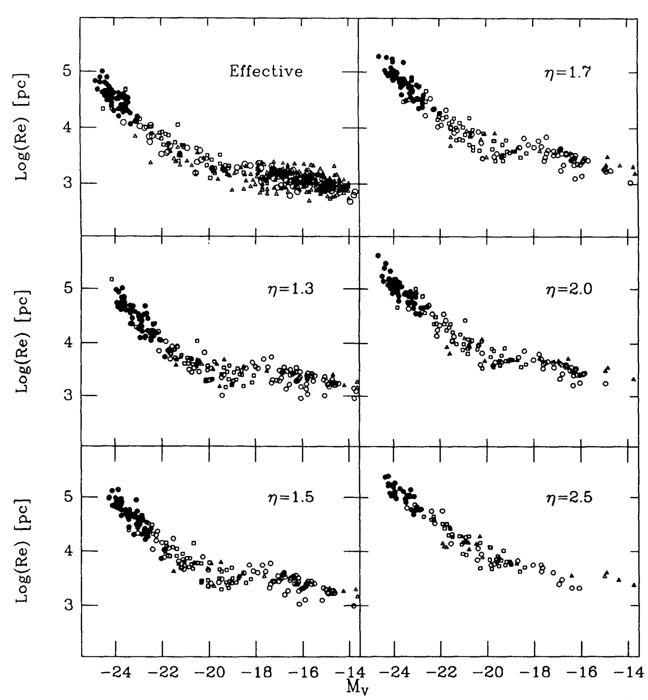

FIG. 2.—Comparison of data for first-ranked galaxies (*closed circles*) from Table 1 with data from Paper II for the Virgo, Fornax, and Coma clusters (*open symbols*) brighter than $M_V = -14$. Effective photometric parameters are used in the upper left panel. Other panels show data for five values of the Petrosian η parameter.

where the first-ranked data in the present study are combined with data for the Virgo and Coma clusters.

Shown in the upper left panel of Figure 2 are the data for "effective" radii and "effective" absolute magnitude. The other panels show the data for various Petrosian η radii. The deviation of the brightest galaxies from the "constant ⟨SB⟩ condition" (which is a straight line of slope 5 shown in Fig. 1) for all E galaxies brighter than about $M_V = -22$ is evident.

Figure 3, similar to Figure 4 of SPII, shows the extension to brighter luminosities of the (R, M) correlation. The first ranked cluster galaxies in Table 1 have been added as closed circles to the data for the Virgo, Fornax, and Coma cluster from SPII. The "effective" linear radius and the total V absolute magnitude are used as the coordinates. Open circles are Virgo Cluster galaxies, open squares are the Coma Cluster, open triangles are for the Fornax Cluster. The line of constant ⟨SB⟩ at 20 mag arcsec^{-2} is shown.

3.2. *Variation of* ⟨*SB*⟩ *with Absolute Magnitude*

Figure 4 shows the data in the ⟨SB⟩, M_V plane using the same symbols as in Figure 3. A most important feature of this diagram is the steepening of the ⟨SB⟩, M correlation at the brightest luminosities compared with the fainter data discussed in SPII (Fig. 11). In Table 6 of SPII the slope is given as $d\langle SB\rangle/dM_V \approx -0.5$ over the magnitude range from $-20 > M_{V(e)} > -23$. In the brighter M interval of $-25 < M_{V(e)} < -23$ in Figure 4 the slope is ≈ -1. The consequences of this very strong variation of ⟨SB⟩ with M (also with R as in § 3.3 below) for first-ranked galaxies is that the correction of ⟨SB⟩ to fixed M is even more vital than for the fainter galaxies in using data for the Tolman test.

The correlation of ⟨SB⟩ with M is shown in more detail in Figure 5 using only data from Table 1. The arrows in each panel are the vectors for errors in apparent magnitudes of 0.5 mag if the radii remain fixed. Note that the errors in each coordinate are coupled. A change of Δm in the apparent magnitude (and therefore in M) causes a change of the same amount in ⟨SB⟩. Because the error vectors are nearly orthogonal to the correlation direction, the *intrinsic* scatter in the true correlation is smaller than the *apparent* scatter shown in Figure 5. This important point shows that ⟨SB⟩ for E galaxies *is a very well defined parameter* with an intrinsic scatter at a given M or R value that is small enough to make the Tolman test practical. The same conclusion was reached in SPII from different data and was a principal conclusion of that paper.

3.3. *Variation of* ⟨*SB*⟩ *with R*

Because of the steep variation of ⟨SB⟩ with M in Figures 4 and 5 and because of the coupling of the error vectors that artificially widen the spread in ⟨SB⟩ at a given M, we inquire if the correlation of ⟨SB⟩ with log R is more suitable than the correlation with M as a correction relation. That the aforementioned problems do not exist in this representation is shown in Figure 6 from the data in Table 1. As before, first-ranked galaxies are shown as closed circles; non–first ranked are open circles.

The equation of the least-squares correlation line calculated using the total sample of 146 galaxies is

$$\langle SB\rangle = 2.81 \log R(\mathrm{pc}) + 10.09 , \tag{1}$$

over the interval $3.8 < \log R(\eta = 2) < 5.4$. The result is obtained by averaging the two calculations made by exchang-

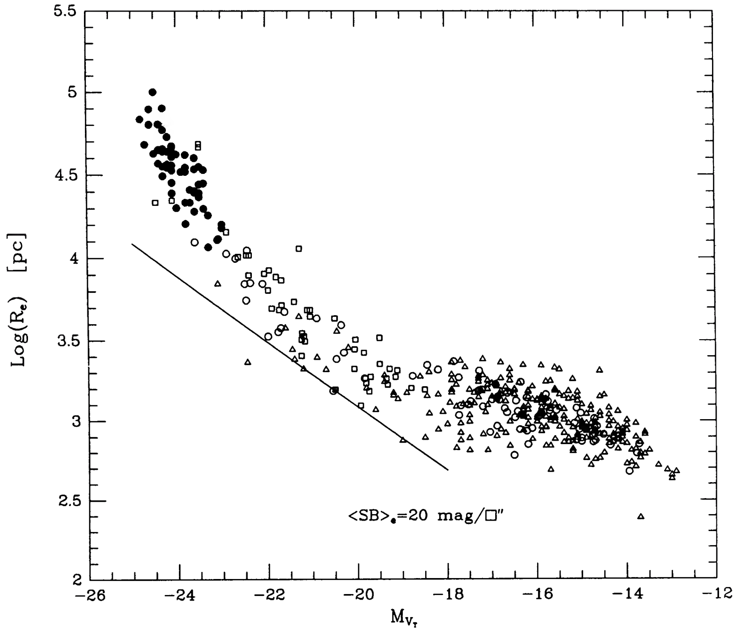

FIG. 3.—Extension to brighter magnitudes of the R_e, $M_{V(\text{total})}$ correlation from Paper II by adding data for first-ranked galaxies (*closed circles*) from the clusters in Table 1. Triangles are galaxies in the Fornax cluster, squares are for Coma, and open circles are for Virgo.

ing ⟨SB⟩ and log R as the independent variable to obtain an approximation to an "impartial" solution (Seares 1944).

Using only the 56 first-ranked galaxies gives a solution that differs slightly from equation (1) because those data exist in a narrower interval of log R, and because the correlation in Figure 6 is slightly nonlinear. The "impartial" solution for first-ranked galaxies alone in Table 1 is

$$\langle SB \rangle = 3.12 \log R(\text{pc}) + 8.51 \; , \qquad (2)$$

over the interval $4.4 < \log R(\eta = 2) < 5.4$.

The dispersions about equations (1) or (2) are 0.35 and 0.27 mag, respectively. These are much smaller than the dispersions either in Figures 4 and 5, or as shown in SPII (Figs. 15 and 16) from the Virgo, Fornax, and Coma cluster samples. The smallness of the dispersion in Figure 6 was a remarkable surprise to us in view of the large total range in ⟨SB⟩ by a factor of 100

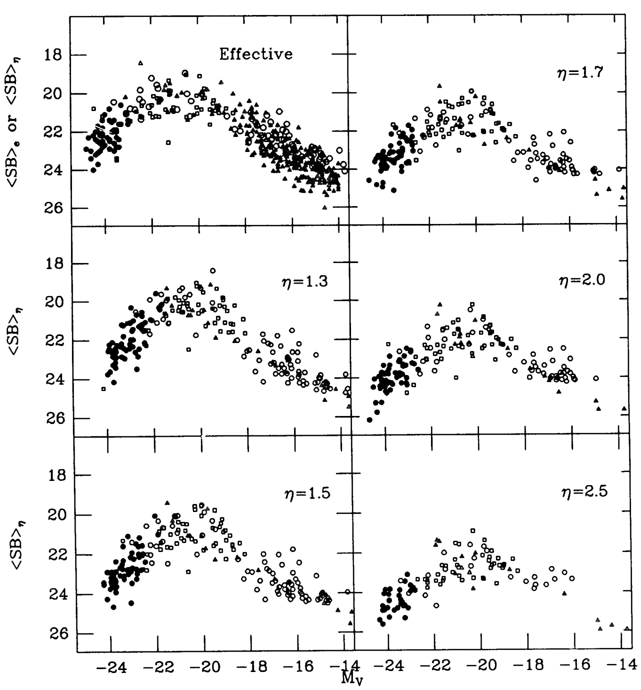

FIG. 4.—Extension to brighter magnitudes of the ⟨SB⟩, $M_{V(\text{total})}$ correlations of Paper II using the first-ranked galaxies in the additional clusters from Table 1. Symbols are the same as in Fig. 3.

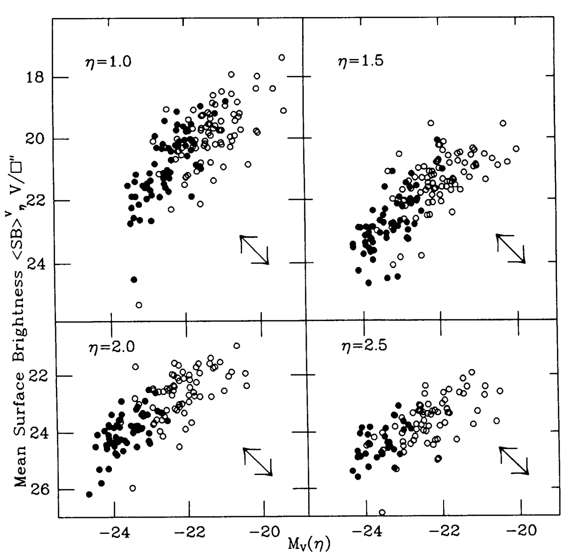

FIG. 5.—The ⟨SB⟩, $M_{V(\eta)}$ correlations for four η values using the data from Table 1. First-ranked galaxies are closed circles; others are open circles. Vectors at the lower right in each panel show the effect of a 0.5 mag error in M, keeping R fixed.

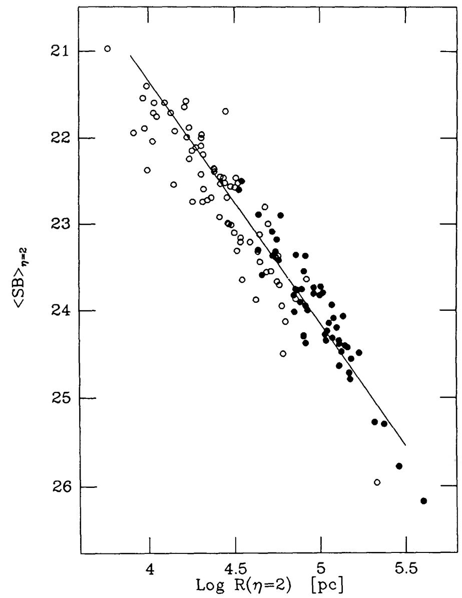

FIG. 6.—Correlation of $\langle SB \rangle^V$ with log R(pc) from the data in Table 1 for $\eta = 2$ mag arcsec^{-2}. Closed circles are for first-ranked galaxies; open circles are for fainter galaxies in the same clusters. The line is the least-squares solution of eq. (1) of the text.

(N.B. $\langle SB \rangle$ varies between 21 and 26 mag arcsec^{-2} for the total sample in Fig. 6).

4. A SELECTION EFFECT THAT IMITATES A TOLMAN SIGNAL

Without knowledge of either Figures 4, 5, or 6 one might have imagined that a search for a Tolman signal could be made using first-ranked galaxies alone (Geller & Peebles 1972) without reductions of the $\langle SB \rangle$ data to "standard conditions." The rationale would be the small dispersion of $\langle M \rangle$ of first-ranked cluster members (Humason, Mayall, & Sandage 1956; Sandage & Hardy 1973 with prior references; Gunn & Oke 1975). But in view of the large variation in $\langle SB \rangle$ with M even among first-ranked galaxies (Figs. 4, 5, and 6) it is clear that such a procedure would work even using averages of large numbers only if no *selection biases* exist in any particular data set.

But all samples contain selection biases, some of which produce an artificial change of $\langle SB \rangle$ with z that imitates the Tolman cosmological effect. The most common bias is an increase in the absolute luminosity of individual galaxies with increasing redshift. This is the famous Malmquist bias that dominates statistical astronomy. The consequence for the present problem is that if, in any particular galaxy sample, $\langle M \rangle$ becomes brighter with increasing z due to selection bias, the steep correlation of $\langle SB \rangle$ with M in Figures 4 and 5 will give $\langle SB \rangle$ values that become fainter with increasing z. This is the same direction as the Tolman effect, but clearly it is not the Tolman cosmological signal but is simply a result of the bias.

A Malmquist increase of mean luminosity of any sample with increased distance is always present if the sample is chosen by apparent magnitude whenever the luminosity function has a finite width. It is simply the effect of the increased normalization factor in the luminosity function with increased volume. Clearly, any Malmquist-like effect must be eliminated if a false Tolman signal is to be avoided. We show later in this section that *the correction to "standard conditions"* does this automatically.

A similar bias that is more common in catalogs of clusters is the Scott (1957) effect due to the apparent change of cluster properties with distance. It is caused by the methods that are used to identify the cataloged clusters. Clusters more distant than others are buried deeper in foreground contamination the greater the distance. As the contamination increases, the fraction of the listed clusters with abnormally bright first few ranked members due to greater than average cluster richness will increase with redshift. The effect is to cause an increase in luminosity of the brightest cluster members with distance due to the biased selection criteria.

A Scott-like effect is present in the data in Table 1 as shown by the (z, m) Hubble diagrams in Figure 7. The least-squares regressions drawn in each panel as the solid lines have nearly identical slopes of $dm/d \log z = 3.8$. These slopes are quite significantly smaller than 5 with which the dashed envelope lines in the diagram have been drawn. The slope of 5 is, of course, the requirement of a linear redshift-distance relation if $\langle M \rangle$ does not vary with distance. The deviation of the solid line from the slope of the envelope lines is the proof that a selection bias affects the absolute magnitudes in the Table 1 data.[4]

That an increase in average cluster richness with distance is the reason for the Scott-like bias in the Table 1 data is shown in Figure 8. The "total" absolute V magnitude listed in the table is plotted in the top panel versus the cluster distance modulus, also from Table 1. The cluster richness listed by Abell (1958) is correlated with distance in the bottom panel. Because the absolute magnitude of first-ranked galaxies brightens with increasing richness (Sandage & Hardy 1973; Sandage 1975, 1976; Sandage, Kristian, & Westphal 1976), the trend shown in the upper panel is understood. In turn, because of the correlation of $\langle SB \rangle$ with M in Figures 4 and 5, this produces a systematic variation of $\langle SB \rangle$ with *z that imitates a Tolman signal*, but the trend is simply an artifact of the Scott bias.

Figure 9 shows the presence of the biasing effect in the data of Table 1 using both the effective and the $\eta = 2$ parameters. The least-squares slopes of the solid line drawn in each panel are the same at $d\langle SB \rangle \backslash d \log (1 + z) = 35.2$. A true Tolman signal would have a slope of 12.5.[5]

[4] The objection to this demonstration would be based on denying an intrinsically linear redshift-distance relation. Two versions of the objection exist. (*a*) To the extent that local random motions perturb an assumed local linear Hubble flow, deviations from $m \sim 5 \log z$ will occur. These, however, should not be progressive with distance beyond redshifts of about $z = 0.02$, and they will tend to average out around the sky. (*b*) In cosmologies that deny a linear Hubble expansion velocity field itself (e.g., Segal 1981), any systematic deviation from a slope of 5 is interpreted by the authors of any nonlinear theory as a deviation of the "true redshift-distance relation" from linearity. We answer by stating that the linear law repeatedly has been shown to be correct using bias-free samples and photometric reduction techniques that *are model independent* (Sandage 1972a, 1973a, b, 1976; Sandage & Hardy 1973, Kristian, Sandage, & Westphal 1978). It further has been shown that apparent deviations from the linear requirement that $m \sim 5 \log z$ are expected (indeed *are required* in the data) due to selection effects in biased samples (Sandage, Tammann, & Yahil 1979) whenever the sample has a broad luminosity function as for field galaxies. The point is that the established linearity of the redshift-distance relation can be used via the deviation in the Hubble diagram for any data sample to *discover* bias properties of the sample (see Sandage 1988a, b).

[5] Recall the $(1 + z)$ bandwidth term in data not corrected for the K dimming term. At the maximum redshift in Table 1 of $z = 0.1$ the *selective* part of the K term in R magnitudes is negligible (because the spectrum over this wavelength interval is flat in $I(\lambda)d\lambda$; Oke & Sandage 1968; Schild & Oke 1971; Pence 1976; Coleman, Wu, & Weedman 1980), justifying the neglect of the K corrections in Figs. 7–9. But the *bandwidth* part of the term must be accounted for in a discussion of the expected Tolman slope if it has not been included in the data. This causes an additional factor of log $(1 + z)$ in the Tolman term in the *observed* $\langle SB \rangle$ value when the photometric data have not been K corrected, giving a total Tolman factor whose slope is 12.5.

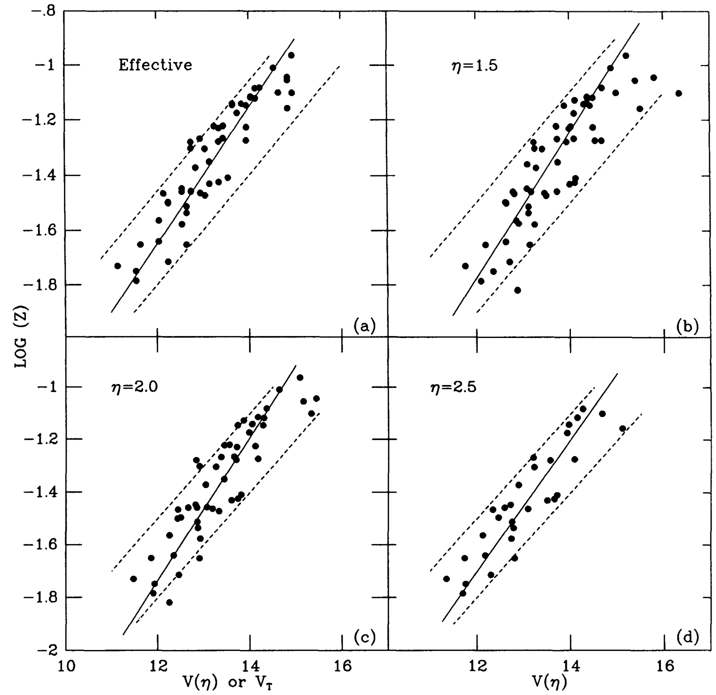

FIG. 7.—The Hubble diagrams using effective V apparent magnitudes and V magnitudes inside three Petrosian radii values. Data are from Table 1. Dashed envelope lines have a slope of $d \log V/d \log z = 5$. Solid least squares regression lines all have slopes of 3.8, indicating a selection effect that makes the absolute magnitudes of the sample galaxies brighter with increasing redshift.

To prove that the correlation with redshift in Figure 9 is the effect of the bias and not a Tolman signal we have reduced the data to "standard conditions" and show that the correlation largely disappears. The results are given in Figure 10 for the $\eta = 2$ case. The top panel repeats the bottom panel of Figure 9. The middle panel shows the result of reducing the observed $\langle SB \rangle$ values to $\langle M \rangle = -24$ using a slope of $d\langle SB \rangle \backslash dM = -0.9$ given by the data in the lower left panel of Figure 5. The lower panel of Figure 10 shows the reduction to $\log R = 5.0$ using the slope of $d\langle SB \rangle \backslash d \log R = 2.81$ from equation (1) of the last section.

The two conclusions from Figure 10 are (1) in both the middle and the lower panel the reduction to standard conditions has eliminated the imitation Tolman effect in the top panel that is due to selection bias. The slope of the reduced correlation in the middle panel is $d\langle SB \rangle/d \log (1 + z) = 10.7$, with an uncertainty large enough to overlap a Tolman slope of 12.5. The slope of the least-squares line in the lower panel is $d\langle SB \rangle/d \log (1 + z) = 0.8$. The dashed line has a Tolman slope of 12.5. It is nearly indistinguishable from the solid line. (2) The dispersion of $\sigma(\langle SB \rangle) = 0.27$ mag in the lower panel is smaller than $\sigma(\langle SB \rangle) = 0.53$ in the middle panel, showing that the $\langle SB \rangle$, R correlation is the stronger route to the "reduction to standard conditions." As mentioned earlier, this is because the correlation in Figure 6 is tighter than in Figure 5 since any error in M widens the spread in Figure 5. Furthermore, R is more accurately determined, in general, than M because it is independent of zero-point errors in the photometry.

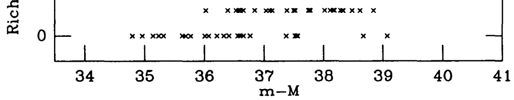

FIG. 8.—Proof that the effect in Fig. 7 is a selection bias. Top panel shows the absolute magnitudes of the galaxies in Fig. 7 in the $\eta = 2$ panel as a function of distance modulus (for $H_0 = 50$) assuming a linear redshift-distance relation. Bottom panel shows the increase in the mean Abell richness parameter with redshift.

The conclusions from this section are (1) it is crucial to eliminate selection biases in any set of data before searching for the Tolman $\langle SB \rangle$ signal; (2) such biases, no matter what their cause, *can* be eliminated by reducing the data to the "standard conditions" of either fixed M or fixed R, and (3) the preferred reduction is to fixed R because (*a*) the required $d\langle SB \rangle/d \log R$ slope is better determined (Fig. 6), and (*b*) errors in R have a smaller effect on the result than errors in M.

In the next section we apply these results to search for a Tolman signal in a data sample that contains clusters at much larger redshifts than those of Table 1, extending the abscissa in Figure 10 by a factor of 4.

5. SEARCH FOR THE EXPANSION SIGNAL USING THE DATA OF DJORGOVSKI AND SPINRAD

Djorgovski & Spinrad (1981, hereafter DS) measured the Petrosian metric radii for $\eta = 2$ for first-ranked galaxies in 25 clusters that span a redshift range from $z = 0$ to $z = 1.1$. The measurements were made on photographic plates (Eastman IIIa-F plates with filter) that approximate the standard R

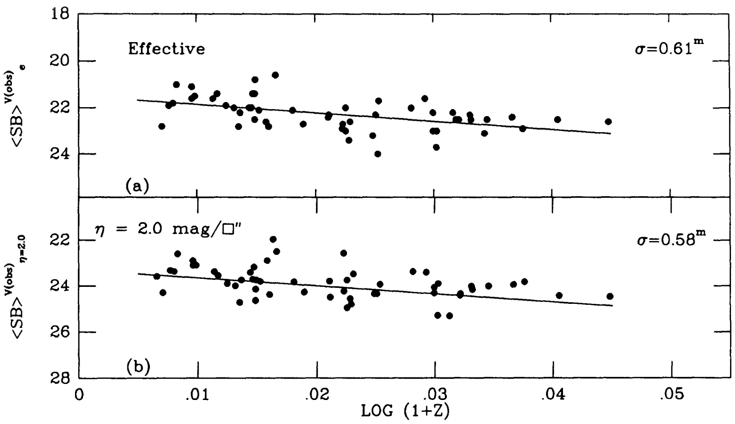

FIG. 9.—Correlations of ⟨SB⟩ with log $(1 + z)$ for the data for first-ranked galaxies in Table 1 using both effective and Petrosian $\eta = 2$ parameters. Each regression line has a slope of $d\langle SB\rangle/d \log (1 + z) = 35.2$. The correlation imitates a Tolman cosmological effect, but with 4 times the expected slope. It is due to the selection bias shown in Figs. 7 and 8 and, hence, is an artifact of the sample.

band. The data were reduced to intensity and zero-point by using a photographic density-intensity calibration in the usual way and assuming a value for the background sky surface brightness (the same for all plates). No additional external photometric standards were used for comparison.

Since Petrosian radii depend only on intensity *ratios* and are therefore independent of magnitude zero-point errors, one would believe that the radii measurements of DS are more accurate than the magnitudes. But the accuracy of the ⟨SB⟩ values depend on both the zero point of the magnitude system and the radii. Therefore, the ⟨SB⟩ values are intrinsically less accurate than the radii. For this reason DS discussed only data for the radii as they relate to the predictions of the standard model (Sandage 1961, 1988c), bypassing thereby the direct ⟨SB⟩ Tolman test.

Nevertheless, their data are in an ideal form to search for the Tolman signal, and we began to do so simply to illustrate the machinery of the corrections we have been discussing. But, remarkably, it soon became evident that a strong Tolman signal exists in the DS data. It has the correct strength if the expansion is real and is statistically significant. We discuss the DS data in this section both to illustrate the reduction procedures and to emphasize again, as in SPII, that the Tolman test is feasible in practice.

The reduction of the DS data are as follows:

The $(m, \log z)$ Hubble diagram using the apparent R magnitudes in Table 1 (col. [10]) of DS is well defined as shown in Figure 11. There is no obvious selection bias; the data, in first approximation, fit the lines, all of which have a slope of $dm\backslash d \log z = 5$ at low redshift, differing in that respect from the data in Figure 7—the circumstance that signals the bias there. The absence of an obvious selection bias and the smallness of the dispersion about the Hubble lines in Figure 11 suggest, then, that a Tolman signal should appear in the data themselves, even uncorrected to standard conditions if, in fact, the Tolman effect exists.

The data are set out in Table 2 for 19 of the DS sample. Six galaxies in the DS sample are not used. NGC 1316 near the Fornax cluster is the radio source Fornax A. It is highly peculiar optically and is not useful as a "standard" galaxy for that

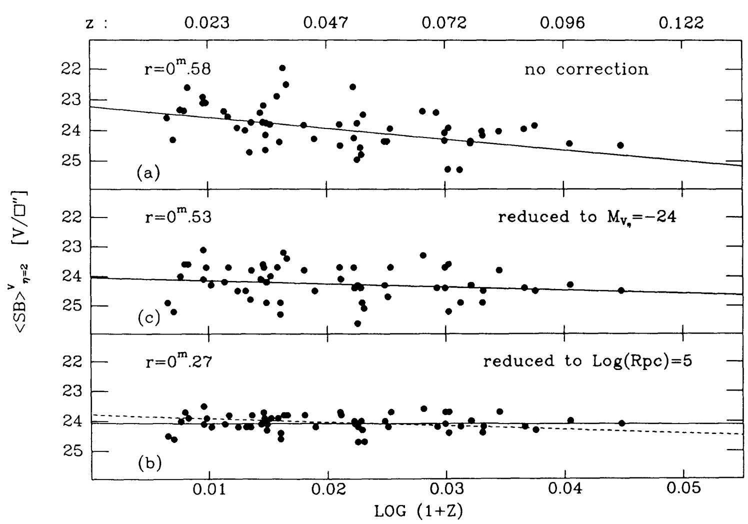

FIG. 10.—The effect on Fig. 9 of reducing the data to the "standard conditions" of $M_V = -24$ and $\log R = 5.0$ using slopes of $d\langle SB\rangle/dM_V = -0.9$ and $d\langle SB\rangle/d \log R = 2.81$. Top panel repeats the second panel of Fig. 9. Middle panel shows the reduction to fixed M. Bottom panel shows the reduction to fixed R. The dispersion of ⟨SB⟩ about the regressions (*solid lines*) are marked. Dashed line in the bottom panel has the slope of 12.5 expected for the Tolman cosmological effect (N.B. no K corrections have been applied to the magnitudes).

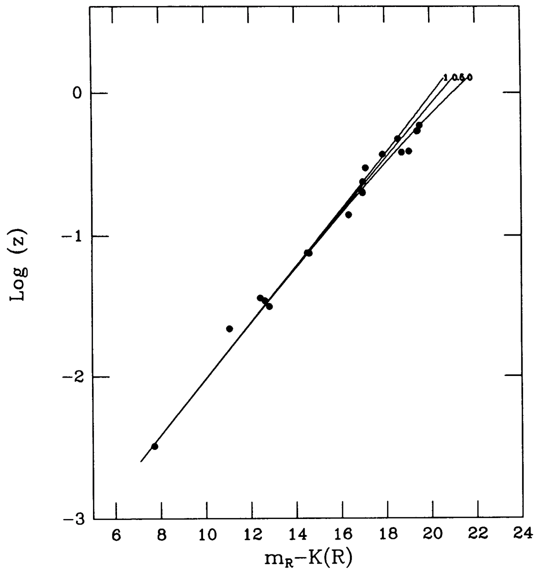

FIG. 11.—The Hubble diagram for the data in Table 2 for the sample of Djorgovski & Spinrad. Lines of constant M for three values of q_0 are shown, calculated from eqs. (3)–(5) of the text.

reason. 3C 295 (Minkowski 1960) is one of the most powerful radio sources known (Sandage 1972b), and its enormous radio energy is suspected of affecting the optical structure (McCarthy 1988, with many references to the earlier work). Similarly, we exclude the powerful radio galaxies 3C 352, 3C 13, and 3C 427.1 and G1 of 1305+2952 at the very large redshifts of 0.806, 1.05, 1.175, and 0.942, respectively, for the same reason as for 3C 295. Because of their peculiarities, we could also suspect that evolutionary effects are more important for them than for galaxies at lower redshift (Djorgovski, Spinrad, & Maar 1985).[6]

We have not used the photometric values given by DS for NGC 4472 in the Virgo cluster because they are not correct. The B_T magnitude from the RSA (Sandage & Tammann 1987) is 9.32. Because $B-R$ colors for nonredshifted E galaxies is 1.8 (Sandage 1973a, Fig. 4; Kristian, Sandage, & Westphal 1978, Figs. 1 and 2), the R magnitude should be 7.52, which value we adopt. The $\eta = 2$ mag arcsec^{-2} radius is taken to be 407″ from the listing in SPII (Table 1).

The data set out in Table 2 are as follows. The redshifts, metric angular radii, and apparent magnitudes are listed in columns (2), (3), and (4), as given by DS. The adopted $K(R)$ correction is in column (5). We assume that the magnitudes in column (4) are on the standard R photometric system (Sandage & Smith 1963; Sandage 1973a) to within the accuracy of that bandpass, so that the standard K correction for R magnitudes can be applied using interpolation and graphical smoothing of Table 6 of Coleman, Wu, & Weedman (1980). This correction includes the bandwidth term of $(1 + z)$. Hence, any Tolman signal that may be present should have a redshift dependence of $(1 + z)^4$ rather than $(1 + z)^5$.

The absolute magnitudes in columns (6)–(8) have been calculated from the K-corrected magnitudes and the redshifts, using assumed values of q_0 and a Hubble constant of 50. The linear

[6] Three (1305, 3C 13, and 3C 427.1) of the five excluded radio galaxies are each ~1.6 mag brighter at their measured redshifts than the theoretical lines in Fig. 11. The redshift and K-corrected magnitude for all five excluded galaxies are (0.461, 17.82) for NGC 295, (0.806, 19.63) for 3C 352, (0.942, 18.16) for 1305+2952, (1.05, 18.45) for 3C 13, and (1.175, 19.37) for 3C 427.1. Although the three galaxies mentioned at the beginning of this footnote deviate from the others of Table 2 in the Hubble diagram of Fig. 11, all five of the strong radio sources show the same tight $r \sim z^{-1}$ angular radius–redshift relation followed by all galaxies in Table 2 (see the diagram in DS). To show the relation again here, the reader can plot the data for the five radio galaxies as (z, r'') sets to be added to the Table 2 data as follows: ($z = 0.461$, $r = 6''.17$) for 3C 295, (0.806, 3″.48) for 3C 352, (0.942, 3″.02) for 1305+2952, (1.05, 2″.2) for 3C 13, and (1.175, 2″.0) for 3C 427.1.

Because the radii of the excluded radio galaxies do not deviate from the $r(z)$ correlation but do deviate from the $m(z)$ lines in Fig. 11, the ⟨SB⟩ of the three excluded galaxies are ~1.6 mag brighter than the mean ⟨SB⟩ correlations in Fig. 12. This presumably is due to evolutionary effects connected with their radio properties that affect the *luminosity of the sources but not their radii*. A follow-up of the obvious implications of this result for an understanding of such evolutionary effects would seem profitable.

TABLE 2

PHOTOMETRIC DATA FROM DJORGOVSKI AND SPINRAD TESTED FOR THE PRESENCE OF A TOLMAN SIGNAL

					M_R^C			log (R pc)				$\langle SB \rangle_R^{C,\ \log(R\ \mathrm{pc})=5}$		
OBJECT (1)	z (2)	r'' (3)	R (mag) (4)	$K(R)$ (mag) (5)	$q_0 = 0$ (6)	$q_0 = 1/2$ (7)	$q_0 = 1$ (8)	$q_0 = 0$ (9)	$q_0 = 1/2$ (10)	$q_0 = 1$ (11)	$\langle SB \rangle_R^C$ (R/arcsec^2) (12)	$q_0 = 0$ (13)	$q_0 = 1/2$ (14)	$q_0 = 1$ (15)
NGC 4472	0.00317	407″	7.52	0.00	−23.68	−23.68	−23.68	4.57	4.57	4.57	22.01	23.20	23.20	23.20
A1367	0.0281	128	11.08	0.02	−24.54	−24.53	−24.52	4.90	4.89	4.89	22.84	23.13	23.14	23.15
A2199	0.0312	40	12.86	0.03	−23.56	−23.55	−23.53	4.54	4.54	4.53	22.08	23.37	23.38	23.39
A1228	0.0344	49	12.67	0.04	−23.98	−23.96	−23.94	4.67	4.66	4.66	22.32	23.25	23.26	23.27
A2151	0.036	54	12.47	0.04	−24.28	−24.26	−24.24	4.73	4.73	4.72	22.33	23.09	23.10	23.11
A401	0.0746	16.4	14.69	0.08	−23.72	−23.68	−23.64	4.50	4.50	4.49	21.93	23.32	23.34	23.36
A2670	0.0753	19.5	14.60	0.08	−23.83	−23.79	−23.75	4.58	4.58	4.57	22.21	23.38	23.40	23.42
A795	0.140	13.34	16.50	0.14	−23.41	−23.33	−23.26	4.65	4.64	4.62	23.23	24.21	24.25	24.29
Hydra II	0.201	5.45	17.19	0.21	−23.64	−23.52	−23.43	4.39	4.36	4.34	21.90	23.62	23.68	23.74
A520	0.203	8.51	17.17	0.21	−23.68	−23.57	−23.47	4.58	4.56	4.54	22.85	24.02	24.08	24.14
Zw 1305	0.240	10.72	17.24	0.25	−24.05	−23.91	−23.80	4.74	4.71	4.69	23.38	24.12	24.19	24.26
Corwin 0404	0.300	8.28	17.44	0.33	−24.47	−24.30	−24.17	4.69	4.66	4.63	22.94	23.80	23.90	23.98
0237−0138	0.373	8.32	18.29	0.42	−24.25	−24.04	−23.88	4.75	4.71	4.68	23.71	24.40	24.51	24.61
0949+4409	0.385	3.55	19.17	0.45	−23.48	−23.27	−23.10	4.39	4.35	4.32	22.71	24.41	24.53	24.63
0024+16	0.392	5.31	19.50	0.46	−23.21	−22.99	−22.82	4.57	4.53	4.49	23.91	25.11	25.23	25.33
PKS 0400	0.480	4.68	19.24	0.68	−24.21	−23.94	−23.74	4.57	4.52	4.47	23.15	24.36	24.51	24.62
0016+16	0.541	5.01	20.20	0.80	−23.68	−23.38	−23.16	4.63	4.57	4.52	24.14	25.19	25.36	25.48
3C 330	0.545	4.37	20.23	0.80	−23.66	−23.37	−23.14	4.57	4.51	4.46	23.88	25.09	25.26	25.39
PKS 0116	0.593	4.22	20.48	0.96	−23.80	−23.47	−23.24	4.57	4.51	4.46	23.89	25.09	25.28	25.41

radii for $\eta = 2$ are in columns (9)–(11), based on the observed radii in column (3) and on the redshift, using the same three q_0 values.

The absolute magnitudes are calculated from the standard Mattig (1958) equations which reduce (Sandage 1988c) to the special cases:

$$M = m - 5 \log [z(1 + 0.5z)] - 43.89 , \quad (3)$$

for $q_0 = 0$,

$$M = m - 5 \log [2(1 + z - (1 + z)^{0.5}] - 43.89 , \quad (4)$$

for $q_0 = 0.5$, and

$$M = m - 5 \log z - 43.89 , \quad (5)$$

for $q_0 = 1$,

assuming $H_0 = 50$ km s^{-1} Mpc^{-1}. The three lines of constant M for different q_0 values shown in Figure 11 are calculated from these equations, adopting $\langle M \rangle = -23.7$ to make the lines in Figure 11 fit the data at small z.

The linear radii in columns (9)–(11) are calculated from the special cases of the general equation given elsewhere (Sandage 1988c, eq. [45]), that for the three cases considered here, reduce to

$$R(\mathrm{pc}) = 2.909 \times 10^4 r('')[z(1 + 0.5z)(1 + z)^{-2}] , \quad (6)$$

for $q_0 = 0$,

$$R(\mathrm{pc}) = 5.818 \times 10^4 r('')[\{(1 + z)^{-0.5} - 1\}(1 + z)^{-1.5}] , \quad (7)$$

for $q_0 = 0.5$, and

$$R(\mathrm{pc}) = 2.909 \times 10^4 r('')[z(1 + z)^{-2}] , \quad (8)$$

for $q_0 = 1$,

where the Hubble constant is again assumed to be 50 km s^{-1} Mpc^{-1}.

The observed mean surface brightness $\langle \mathrm{SB} \rangle$ in the R band corrected for K dimming is given in column (12), calculated from the data in columns (3), (4), and (5). Finally, columns (13)–(15) show the $\langle \mathrm{SB} \rangle$ values from column (12) reduced to the "standard condition" of $\log R = 5.0$, using the slope of the $\langle \mathrm{SB} \rangle$, R correlation to be $d\langle \mathrm{SB} \rangle / d \log R = 2.81$ from equation (1).

The data from columns (12)–(15) are shown in Figure 12 where $\langle \mathrm{SB} \rangle$ is correlated with $\log (1 + z)$. The top left panel shows the data from column (12), corrected for K dimming but not reduced to $\log R = 5.0$. The solid line is the least-squares regression that uses $\langle \mathrm{SB} \rangle$ as the independent variable. Its slope is $d\langle \mathrm{SB} \rangle / d \log (1 + z) = 8.9 \pm 1.5$. The dispersion about the solid line is $\sigma \langle \mathrm{SB} \rangle = 0.44$ mag which is similar although somewhat less than shown in Figure 10 (*middle panel*) for the first-ranked galaxies in the local clusters. The dashed line is the expected correlation of slope 10.0 if a Tolman true expansion signal is present.

The remaining panels show the result of reducing the $\langle \mathrm{SB} \rangle$ data to $\log R = 5.0$ in the manner discussed above for different q_0 values. We emphasized in SPII that the "reduction to standard conditions" depends only very slightly on the value of q_0. This is demonstrated in Figure 12. The slopes of the three correlations for q_0 values of 0, 0.5, and 1 are very similar at $d\langle \mathrm{SB} \rangle / d \log (1 + z)$ of 9.9, 10.8, and 11.5, respectively, each with a probable error of ± 0.92. Therefore all are in agreement with the prediction of a slope of 10 from the standard cosmological model in which the universe expands.

The equations of the least-squares lines using the data from Table 2 reduced to $\log R = 5.0$ in Figure 12 are

$$\langle \mathrm{SB} \rangle_R^c = 9.90 \log (1 + z) + 23.11 , \quad (9)$$

for $q_0 = 0$,

$$\langle \mathrm{SB} \rangle_R^c = 10.79 \log (1 + z) + 23.11 , \quad (10)$$

for $q_0 = \frac{1}{2}$,

$$\langle \mathrm{SB} \rangle_R^c = 11.50 \log (1 + z) + 23.11 , \quad (11)$$

for $q_0 = 1$.

In addition to the results in Figures 12*b*–12*d*, remarkable if true, the other most satisfactory feature of Figure 12 is the dramatic reduction of the scatter of the reduced data about the correlation lines in the last three panels. The dispersions there are all $\sigma \langle \mathrm{SB} \rangle = 0.27$ mag. This small value is identical with the dispersion in surface brightness for the first-ranked cluster members in Table 1, as reduced to fixed R in the last panel of Figure 10. The similarity of the scatter in these two dissimilar samples and the dramatic effect of reducing to a fixed R give

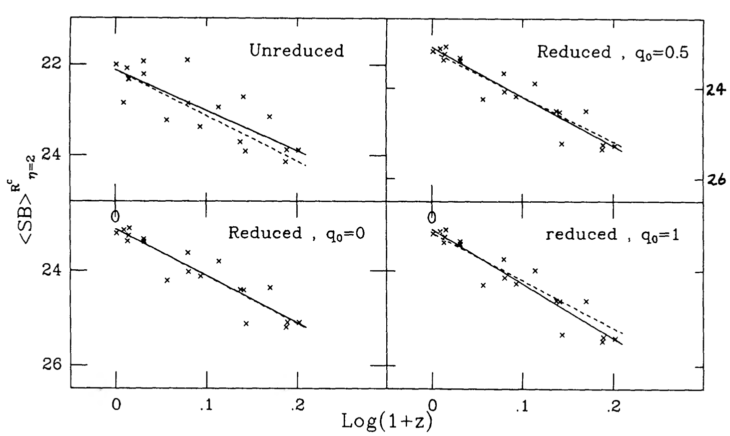

FIG. 12.—Correlation of $\langle \mathrm{SB} \rangle$ with $\log (1 + z)$ for the galaxies in Table 2 from the sample of Djorgovski & Spinrad. The data are not reduced to "standard conditions" in the upper left panel. The data reduced to $\log R = 5.0$ via eq. (1) of the text are in the remaining panels for three values of q_0, showing the virtual independence of the reduction machinery to the value q_0. The solid line in each panel is the least-squares regression of $\langle \mathrm{SB} \rangle$ on $\log (1 + z)$, calculated using $\Delta \langle \mathrm{SB} \rangle$ residuals. Dashed lines have a slope of $d\langle \mathrm{SB} \rangle / d \log (1 + z) = 10.0$ expected for the Tolman cosmological effect. Note that the range of the abscissa here is 4 times greater than in Fig. 10.

reasons to believe that the correction procedure given here is effective.[7]

Yet satisfactory as these results seem for the standard model and, by consequence, for the conventional interpretation of the redshifts, the reliability of the demonstration must be questioned on several grounds.

1. As emphasized by DS, the photometry from their Table 1 should be improved. It is, of course, certain that no errors exist in any of their R magnitude zero points that would be large enough to *erase* the observed 2 mag decrease in $\langle SB \rangle$ over the range of 0.2 dex in $(1 + z)$ shown in Figure 12. The maximum error in using their method via the sky brightness in any field to estimate the zero points of their magnitude system is likely to be less than 0.2 mag (see note 7). Nevertheless, the determination of an exact value for the $d\langle SB \rangle/d \log (1 + z)$ slope, important for the Tolman test, is compromised by photometric uncertainties that can be reduced with new data for individual clusters.

2. The smallness of the sample is unsatisfactory; consequently, the generality of the decrease in $\langle SB \rangle$ in Figure 12 at high redshifts is yet to be proved using a larger sample.

3. The effect of evolution, both passive and active, is yet to be sufficiently demonstrated to either put the problem to rest or to account for it by a correction procedure. As discussed in SPI and in the Introduction here, the expected passive evolution caused by the main-sequence termination point burning down with time is believed to be small compared with the Tolman signal, being only $\Delta M \sim 2.5 \log (1 + z)$. Furthermore, the sense of this type of evolution is to *increase* the luminosity (and hence the SB if R remains fixed) with increasing z, opposite the trend in Figure 12. If such evolution is present, the expected slope of the lines in Figure 12 would then be ~ 7.5 rather than 10. To test for this effect we need a much larger sample at large redshift than is used here.

4. A new sample could be chosen to minimize effects of different types of evolution, following, for example, the selection method used by Hamilton (1985). This would eliminate galaxies with episodes of active evolution. It will be especially important to avoid galaxies that are strong radio sources. Such was not possible at the time DS made their study because nearly all the high-redshift galaxies then known had been found in radio source identification programs. Modern non-radio surveys for distant clusters have changed that.

5. To avoid the postulated evolutionary effects if cannibalism in the first ranks exists (Hausman & Ostriker 1978), a number of galaxies in each cluster fainter than the brightest several should be studied to sample the larger parameter range in Figures 4–6.

In view of these several ways to verify and/or improve the data, we retain an open option on whether the Tolman effect has, beyond doubt, been found, strong as the evidence appears in Figure 12. In addition to the points in the preceding paragraphs, there are other technical ways to improve a definitive Tolman test.

6. THE REQUIREMENTS FOR MAKING A DEFINITIVE SURFACE BRIGHTNESS TEST

A major improvement can be made in the character of the data at large redshifts by using the modern CCD detectors. We would like to monitor the effects of evolution on the spectral energy distribution (SED) and also to improve the technical correction for the effect of redshift on the measured magnitudes (the K term). Both can be accomplished if the photometry is done by including data from low-resolution spectra in addition to those obtained in broad-band imaging.

Ideally, photometry of the spectrum should be performed over the proper (rest) wavelengths simply by moving the analyzed wavelength range in step with the redshift. Evolution, which in the past has been simply ignored or has been estimated theoretically, could also be monitored. Its presence would be presumably be signaled by any change in the 4000 Å break (Bruzual 1983; Hamilton 1985; Spinrad 1986; Dressler & Shectman 1987; Kimble, Davidsen, & Sandage 1989), and/or by departures from a standard SED at high redshift for otherwise "normal" E galaxies. The extreme form of this type of evolution would be the E + A phenomenon of Dressler & Gunn (1982, 1983). Even evidence of mergers could be seen in the spectra (differences in the hydrogen absorption line strength relative to continuum colors) if S and E galaxy types coalesce as cannibals among the first-ranked cluster galaxies.

In summary, the new steps to make a definitive search for the Tolman signal are the following:

1. Assemble a large list of galaxy clusters with redshifts that range from 0 to 1, chosen from optical rather than radio surveys.

2. Obtain low-dispersion spectra (resolution of $\lambda/\Delta\lambda \sim 50$ is sufficient) over the observed range of 3800–20,000 Å, and over large enough fractions of each galaxy's image to map (or to account for) the expected radial gradients in the SED. The spectra are to be used to monitor evolution and to provide the data for each galaxy to convert the imaging photometry, mentioned next, to the proper (rest) wavelengths for each redshift. (Note that unless the spectra themselves are two-dimensional, an imaging part to the experiment is necessary, making the photometric K correction again necessary).

3. In the absence of two-dimensional spectra over the entire galaxy image, one must obtain two-dimensional photometry of many galaxies in each cluster. From these, measure Petrosian radii and magnitudes inside these radii at various η values, calculating therefrom $\langle SB \rangle(\eta)$ values at each observed broad bandpass used. Obtain these data for a large enough sample in each cluster to explore a significant range of the parameter space in Figures 4–6. The purpose is to monitor adequately the correlations in these diagrams, preparatory to their use in "reducing the data to standard conditions." Imaging and data reduction in *two* bandpasses is desirable as a check of the K-corrected data. The final answer must be the same for both data sets because the Tolman effect is wavelength independent.

[7] It is of interest to put the data from Fig. 10c for the "local" galaxies into Fig. 12 by changing the zero point of the photometric system from the V band to the R band. As mentioned in the text, the mean color of E galaxies is $B-R = 1.8$ mag at $z = 0$. It is also known that $B-V = 1.0$ for such galaxies. Therefore, $V-R = 0.8$ mag, V being fainter than R. Hence, $\langle SB \rangle_V - \langle SB \rangle_R = 0.8$ mag, R values being brighter. Subtracting 0.8 mag from the zero point of $\langle SB \rangle_V = 23.9$ at $z = 0$ in Fig. 10 (making it brighter) gives $\langle SB \rangle_R = 23.1$ as the "local" cluster galaxy (from Table 1) $\langle SB \rangle$ expectation at $z = 0$.

The exact agreement of this "local" cluster zero point from Fig. 10c with the constant term in eqs. (9)–(11) for the DS remote cluster data is of considerable interest. Clearly, the data in Fig. 10c fit precisely into the correlations of Figs. 12b–12d over the redshift range of $0 < \log (1 + z) < 0.05$, adding considerable weight to the calibration of the surface brightness relation at the low redshift end. Besides strengthening this needed local calibration for any new attempt to make the Tolman test with a new sample at high redshifts, this agreement also shows (1) the high reliability of the DS photometric zero point value in the R band and (2) gives confidence in the methods of measuring surface brightness values and the corrections of these values to standard conditions to remove selection bias effects using the methods developed in this series.

4. After correcting for evolution (if necessary), make the reductions to fixed M or fixed R using the correction procedures in this series. Seach then for the Tolman signal in the reduced data. If it is found, the universe expands, and the conventional interpretation of the redshift would be correct. The result, strangely enough, would be contrary to an expectation of Hubble (1936, 1938, 1953) where he kept open the possibility that the universe does not expand.

We are grateful to James Schombert, Augustus Oemler, Patricia Vader, and L. Vigroux for generously supplying their radial profile data in digital form from which the calculations for this and for earlier papers of the series were made. Both of us are also grateful to the Physics and Astronomy Department of the Johns Hopkins University and the Space Telescope Science Institute for financial and facility support during 1987–1988 when the initial work on this project was done. J.-M. P. acknowledges fellowship and other support from the Department of Physics and Astronomy during the subsequent years required for the completion of the series. A. S. thanks the Carnegie Institution of Washington for the same reason.

REFERENCES

Abell, G. O. 1958, ApJS, 3, 211
Arimoto, N. 1989, in Evolutionary Phenomena in Galaxies, ed. J. E. Beckman & B. E. J. Pagel (Cambridge: Cambridge University Press), 323
Bruzual, A. G. 1983, ApJ, 273, 105
Coleman, G. D., Wu, C.-C., & Weedman, D. W. 1980, ApJS, 43, 393
Djorgovski, S., & Spinrad, H. 1981, ApJ, 251, 417
Djorgovski, S., Spinrad, H., & Maar, J. 1985, in Lecture Notes in Physics, Vol. 232, New Aspects of Galaxy Photometry, ed. J. L. Nieto (Berlin: Springer), 193
Dressler, A., & Gunn, J. E. 1982, ApJ, 263, 533
———. 1983, ApJ, 270, 7
Dressler, A., & Shechtman, S. 1987, AJ, 94, 899
Geller, M. J., & Peebles, P. J. E. 1972, ApJ, 174, 1
Gunn, J. E., & Oke, J. B. 1975, ApJ, 195, 255
Hamilton, D. 1985, ApJ, 297, 371
Hausman, M., & Ostriker, J. A. 1978, ApJ, 224, 320
Hoessel, J. G., Gunn, J. E., & Thuan, T. X. 1980, ApJ, 241, 486
Hubble, E. 1926, ApJ, 64, 321
———. 1936, ApJ, 84, 517
———. 1938, Observational Approach to Cosmology (Oxford: Oxford University Press)
———. 1953, MNRAS, 113, 658
Humason, M. L., Mayall, N. U., & Sandage, A. 1956, AJ, 61, 97
Kimble, R., Davidsen, A., & Sandage, A. 1989, ASpSc, 157, 237
Kormendy, J. 1977, ApJ, 218, 333
Kristian, J., & Sachs, R. K. 1966, ApJ, 143, 379
Kristian, J., Sandage, A., & Westphal, J. A. 1978, ApJ, 221, 383
Longo, G., & de Vaucouleurs, A. 1983, UTexPAs, No. 3
———. 1985, UTexPAs, No. 3A
Malumuth, E. M., & Kirshner, R. P. 1985, ApJ, 291, 8
Mattig, W. 1958, ANach, 284, 109
McCarthy, P. J. 1988, Ph.D. thesis, University of California, Berkeley
Minkowski, R. 1960, ApJ, 132, 908
Oemler, A. 1974, ApJ, 194, 1
———. 1976, ApJ, 209, 693
———. 1987, in Stellar Populations, Proc. Workshop Space Telescope Science Institute, ed. A. Renzini & M. Tosi (Cambridge: Cambridge University Press), 197
Oke, J. B., & Sandage, A. 1968, ApJ, 154, 21
Pence, W. 1976, ApJ, 203, 39
Sandage, A. 1961, ApJ, 133, 355
———. 1972a, ApJ, 178, 1
———. 1972b, ApJ, 178, 25
———. 1973a, ApJ, 183, 711
———. 1973b, ApJ, 183, 731
———. 1975, ApJ, 202, 563
———. 1976, ApJ, 205, 6
———. 1988a, ApJ, 331, 583
———. 1988b, ApJ, 331, 605
———. 1988c, ARAA, 26, 561
Sandage, A., & Hardy, E. 1973, ApJ, 183, 743
Sandage, A., Kristian, J., & Westphal, J. A. 1976, ApJ, 205, 688
Sandage, A., & Perelmuter, J.-M. 1990a, ApJ, 350, 481 (SPI)
———. 1990b, ApJ, 361, 1 (SPII)
Sandage, A., & Smith, L. L. 1963, ApJ, 137, 1057
Sandage, A., & Tammann, G. A. 1987, A Revised Shapley-Ames Catalog of Bright Galaxies (Carn IWP, No. 635)
Sandage, A., Tammann, G. A., & Yahil, A. 1979, ApJ, 232, 352
Schild, R., & Davis, M. 1979, AJ, 84, 311
Schild, R., & Oke, J. B. 1971, ApJ, 169, 209
Schneider, D. P., Gunn, J. E., & Hoessel, J. G. 1983, ApJ, 264, 337
Schombert, J. M. 1986, ApJS, 60, 603
———. 1987, ApJS, 64, 643
Scott, E. L. 1957, AJ, 62, 248
Seares, F. H. 1944, ApJ, 100, 255
Segal, I. 1981, Proc. Nat. Acad. Sci., 77, 10
Spinrad, H. 1986, PASP, 98, 269
Tolman, R. C. 1930, Proc. Nat. Acad. Sci., 16, 511
———. 1934, in Relativity Thermodynamics and Cosmology (Oxford: Oxford University Press), 467
Thuan, T. X., & Gunn, J. E. 1976, PASP, 88, 543
Thuan, T. X., & Romanishin, W. 1981, ApJ, 248, 439
van den Bergh, S. 1978, PASP, 89, 746
———. 1988, JRASC, 82, 13